Review Article

Mohammed Asmael, Babak Safaei*, Omer Kalaf, Qasim Zeeshan, Fadi Aldakheel*, Tauqir Nasir, and Zhicheng Yang

Recent developments in tensile properties of friction welding of carbon fiber-reinforced composite: A review

Abstract: In this review article, the joining of carbon fiber-reinforced polymer composite with metallic materials by using friction welding techniques was discussed and the effects of process parameters on the weld properties were evaluated. Major parameters involved in this process were plunge depth (PD), dwell time, joining time, and tool rotational speed. A successful friction joint of carbon fiber-reinforced poly composite laminate (CF-PPS)-metal was formed with an interlayer film of additional polyphenylene sulfide. In addition, a detailed overview of the friction techniques was discussed, such as friction stir spot welding (FSSW), friction stir welding (FSW), and refill friction stir spot welding (RFSSW). In this current work, we had focused on the parameters, process, and their development during friction welding of similar and dissimilar metals with CFRP joint. Regarding the FSSW review, the best tensile shear load was 7.1 kN obtained from AA5182 and CFRP at a rotational speed of 3,000 rpm and 5 s welding time. The thickness for AA5182 and CFRP are 1.2 and 3 mm, respectively. The most efficient parameters are rotational speed, PD, dwell time, and shoulder penetration depth. In addition, the heat generated during the process parameters, its influence on mechanical and microstructure properties along with the possible defects and internal cracks of the similar and dissimilar welded joints will be reviewed and discussed.

Keywords: friction welding, microstructures, carbon fiber-reinforced composite, interlayer, parameters

List of abbreviations

AZ	adhesion zone
CF-PPS	carbon fiber-polyphenylene sulfide
CFRP	carbon fiber-reinforced polymer
FSW	friction stir welding
FSSW	friction stir spot welding
FW	friction welding
HAZ	heat affected zone
JP	joining pressure
JT	joining time
PD	plunge depth
PDZ	plastically deformed zone
PRZ	pin refilling zone
RFSSW	refill friction stir spot welding
RSW	resistance spot welding
SCF/PEEK	short carbon fiber polyether ether ketone
SEM	scanning electron microscope
SSZ	sleeve stirring zone
SZ	stirring zone
T_m	melting temperature
TZ	transition zone

* **Corresponding author: Babak Safaei,** Department of Mechanical Engineering, Eastern Mediterranean University, Famagusta, North Cyprus via Mersin 10, Turkey; Department of Mechanical Engineering Science, University of Johannesburg, Gauteng 2006, South Africa, e-mail: babak.safaei@emu.edu.tr
* **Corresponding author: Fadi Aldakheel,** Institute of Continuum Mechanics, Leibniz Universität Hannover, 30823 Garbsen, Germany, e-mail: aldakheel@ikm.uni-hannover.de
Mohammed Asmael, Omer Kalaf, Qasim Zeeshan, Tauqir Nasir: Department of Mechanical Engineering, Eastern Mediterranean University, Famagusta, North Cyprus via Mersin 10, Turkey
Zhicheng Yang: College of Urban and Rural Construction, Zhongkai University of Agriculture and Engineering, Guangzhou 510225, China

1 Introduction

Carbon fiber-reinforced polymer (CFRP) composite materials are finding increased applications in many areas. They are strong, light, and have a usage in aerospace as well as in automotive industry, where high strength-to-weight ratios

are required. Composite materials considered are very attractive in this industry, due to their high strength, density to stiffness ratio, and excellent physical characteristics. CFRPs class of composite materials are getting more interest in lightweight structures [1–5]. Plastics and metals have a huge difference in chemical and physical properties, thus obtaining bonding between metal and plastic materials is more difficult [6,7]. Although the use of various materials is beneficial in different structures, establishing a joint between dissimilar materials such as composites and metal alloys is a difficult task [8–11] due to their different physicochemical properties [12–16]. Because of their excellent electrical, thermal, and mechanical properties, CFRPs are commonly applied in the fabrication of polymer–matrix composites [11,17–20]. Therefore, extensive research has been performed on the application of conventional pitch-based CFRP in improving and optimizing the characteristics of a wide variety of structures [21–24]. CFRP industry is developing by the constant growth of demand from defense and aerospace as well as small markets such as construction materials and sporting goods [24–27]. In terms of manufacturing composite/metal structures, stack-up construction is an effective joining method. It poses a huge capital cost in structural completion in terms of labor intensiveness [28–31]. Friction welding (FW) is a joining method for solid materials, which creates material coalescence under compressive force when work pieces are moved or rotated relative to each other [32,33], producing heat and plastically displacing material from faying interface [34,35]. The welded joint has a narrow heat-affected zone (HAZ) [36,37], due to high temperature and pressure during

the process, material show plastic deformation in the absence of a fusion zone [38,39]. In the last few decades, FW has been considered a major development in joining materials and has been applied in shipbuilding, high speed rail, aerospace, and automotive industries [40,41].

The state-of-the-art welding techniques for polymers such as laser and ultrasonic welding are consolidated technologies. However, their applications are restricted to certain types of polymers. The FW technique has many advantages over other available joining techniques, including low power consumption, short welding time with high mechanical performance, and low peak temperature and plastic deformation [42]. Liu *et al.* [43] studied FW, that only has a rotational shoulder, to join monomer casting nylon (MC Nylon-6) and 6061-T6 Al alloy. Ratanathavorn and Melander [44] applied FW to join AA6111 and poly-phenylene-sulfide (PPS) at the upper and lower sides. They stated that mechanical interlocking attributes to tensile shear properties.

In many industrial applications, such as wind power towers [45,46], bridge construction [47,48], and in transportation [49,50], lightweight structures are becoming highly popular [51,52]. Aluminum (Al) has a long and successful history of application in the designing, assembling, fabricating, and recycling of different structures with constant growth [53–55], as shown in Figure 1. Currently, numerous well-known automotive companies use this material. Also, other industries such as trim and cosmetic pieces which are available in the aftermarket as well as underbody structures, A-pillars, spoilers, drive shafts, various body panels, and other low-volume, high-performance cars use this material [56,57].
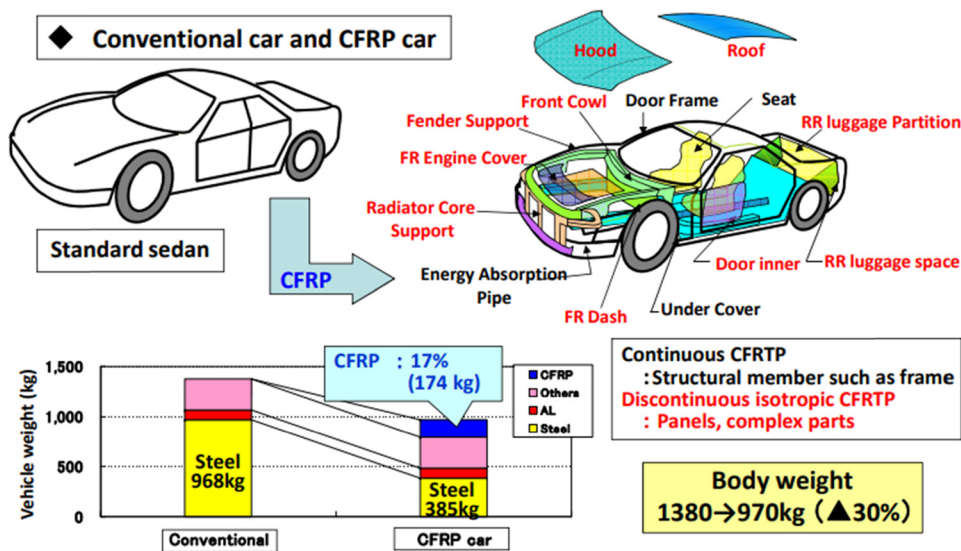

Figure 1: Application of CFRP can reduce body weight by 30% [58].

The application of composite materials in commercial aircraft has become attractive since they reduce the weight of the airframe decreasing fuel consumption and therefore, operation cost [59]. Hereby composite materials accounting for about 50% of the material used in the production of the Boeing 787 can reduce its average weight by 20%. Composite materials are applied in key structural components of several modern helicopters, in which composites comprise about 50% of the total weight as shown in Figure 2. The formability property of the composite materials has been employed in helicopter manufacturing to decrease the number of components and consequently cost [60,61].

Friction heating has been applied in thermoplastic matrix localized melting [63–66]. The abovementioned thermal method depends on matrix material partial melting within CFRPs, resulting in the interlocking and bonding of adhesive to the surface of the metal [67–70]. Several researchers have studied different splicing techniques of metal and plastic materials such as ultrasonic spot welding (USW) [71,72] and FW [73,74]. Generally, mechanical fastening and adhesive bonding [74–76] are the most commonly applied approaches for joining metals and plastic materials [77–79]. Mechanical fasteners increase the weight of a structure and create stress concentration, while the joint fabricated with adhesive bonding requires high surface pretreatment and longer curve times are additional drawbacks [80,81]. Commonly used approaches for joining metals and carbon fiber-reinforced polymers CFRPs, such as adhesive bonding, riveting, bolting, *etc.*, are non-thermal

processes while welding is a thermal process [82–84]. Few research works have been performed on joining matrix composites and metal. However, in some studies, friction stir spot welding (FSSW) has been employed to form an *in-situ* metal matrix composite during welding [85,86]. Normally, polymer materials are joined by adhesives or fasteners. The thermoplastic (plastic polymer) or composite could be successfully joined with metals by FW and achieve the best results [87–89]. However, conventional FSSW provides a convenient and fast alternative for these methods [90] and has been applied to join polypropylene, dissimilar polymethyl, high-density polyethylene [91,92], and methacrylate [93] to acrylonitrile butadiene sheets [94]. In recent years, refill friction stir spot welding (RFSSW) has also been employed to join polymethyl-methacrylate plates and strengths similar to ultrasonic welding or adhesively bonded areas were achieved [95,96]. The aim of this article is to focus on the tensile properties of FW such as FSSW, RFSSW, and friction stir welding (FSW) and also present joints of CFRP with metal and non-metal in different welding processes. Metals and non-metals are different types of materials present around us. Elements can be divided into metals and non-metals and it is important to know whether a particular element is a metal or non-metal. Metals (like copper and Al) are good conductors of heat and electricity, while non-metals (such as phosphorus and sulfur) are insulators. Materials are distinguished as above, based on their properties. The main purpose of this review article is to highlight the latest possible joining methods which can be reliable to join CFRP with metals,
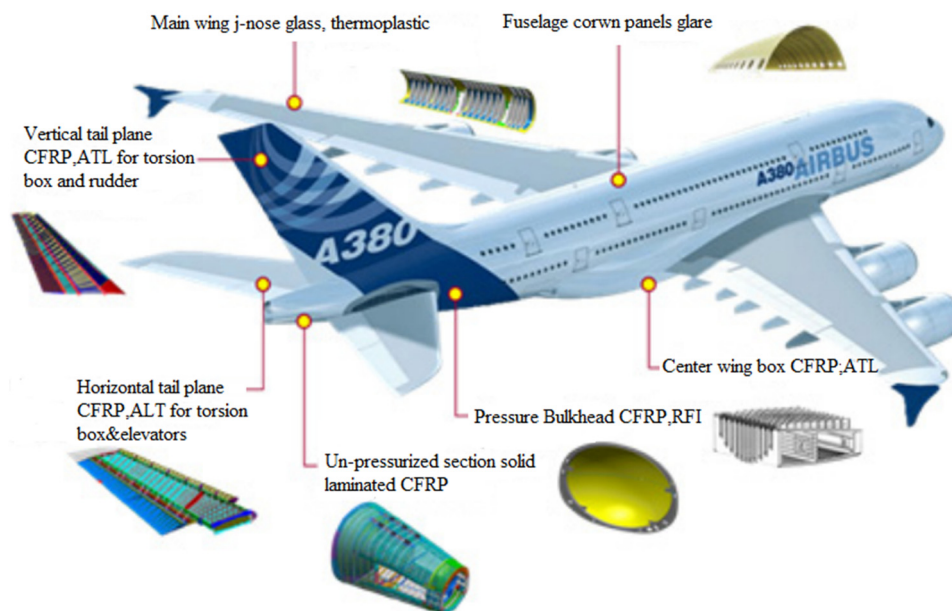

Figure 2: The AIRBUS A380 aircraft composite applications [62].

instead of fasteners and adhesive bonding which cause serious issue and increase extensive weights in structure. FW is a good alternative joining method that can help to weld dissimilar metals without melting any material to create a sound weld joint. This article is organized as follows: Section 1 provides a brief introduction and application of FW. In Section 2, we outline the classification of FSSW and its application and recent progress in this field. In Section 3, RFSSW and its tabular comparison with FSSW are presented. In Section 4, FSW is described and the last section provides the summery about all FW techniques and highlights the significant parameters that affect the strength of weld joint.

2 Methodology

In this review article, the database of articles was collected from different reliable sources like ScienceDirect, Google Scholar, and Scopus. The main sources of articles were Scopus. The articles were searched according to the keywords "friction stir spot welding; refill friction stir spot welding; and friction stir welding, with carbon fiber." The articles published with the keyword of friction stir spot welding were 61. Similarly, the articles published on Scopus with the keyword of refill friction stir spot welding were 12. The total collected articles under the keyword of friction stir welding were 327, published from 2010 to 2022 as shown in Figure 3. Generally, these documents included research papers of more than 70%, conference papers from 5 to 11%, and review papers of about 10%.
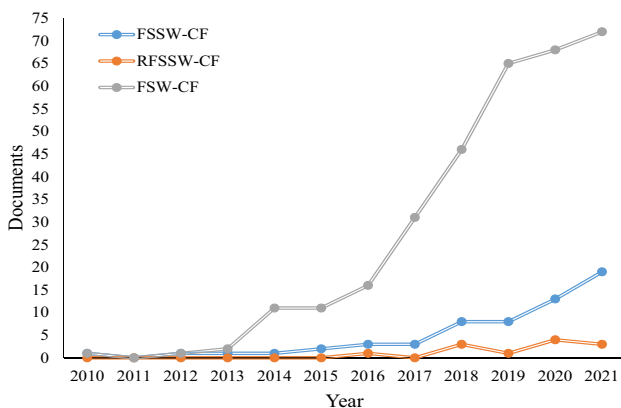
3 FSSW of CFRP

Generally, FSSWs are formed by the retraction of a rotating tool and plunging into and out of the materials to be joined. A keyhole is formed at the end product which is generated by this approach [10,97,98]. FSSW usually takes 2–5 s and during this short time, heat formation in the sheathing case and flipping region links the contacting plates. The energy density created by tool rotation is very high during spot welding [99–101]. FSSW uses a non-consumable tool and generates heat by friction. The tool consists of a sleeve clamping ring and pin which move relative to each other independently and collectively axially [102]. In FSSW, heat is needed and is generated between work pieces and parts. The rotation between sleeve and pin is independent and the parts being joined are held with the ring [103,104]. The rotating sleeve is plunged into the work piece to a predetermined depth while the pin rises. Temperature increases due to the friction between the sleeve and work piece to locally plasticize as shown in Figure 4. Then, the molten layer consolidates under pressure inducing adhesion and snarl between materials and composites [105,106]. Unlike FSW, in FSSW, the tool is plunged up to 40% of the thickness of metal and does not reach composites [107].

The key factor in the generation of heat is tool rotation [109,110], because tool torque is responsible for almost the total energy generated in FSSW [111,112], which also controls material stirring around the tool. The torque of the tool is also responsible for heat generation and thermal cycle [113] and the increase in rotation rate increases temperature resulting in higher mixing
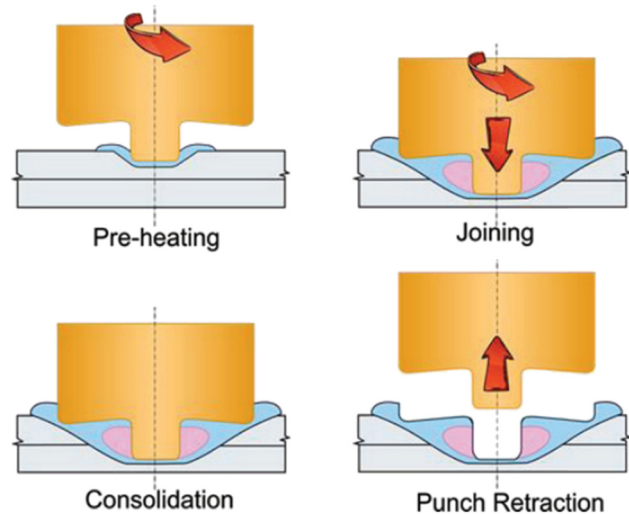

Figure 3: Published documents per year with keywords "friction stir spot welding, refill friction stir spot welding, and friction stir welding with carbon fiber."

Figure 4: Schematic diagram of FSSW process [108].

intensity of the materials. This additional energy input directly relates to weld strength and bonded area [98,114,115]. Sheet thickness and pin length determine tool penetration depth into the contact sheets, which are the most effective factors in weld strength and bond dimensions. The macro-structure of the FSSW weld is highly related to the depth of the shoulder plunge. By the increase in the depth of shoulder plunge, the stirring zone is expanded and material flows upward from the lower sheet [116]. The shoulder penetration has to be deep enough to guarantee horizontal alignment of the interface tip to avoid fracture by the interfacial fracture [117]. However, the tensile shear load is bilaterally affected by the depth of shoulder penetration; a great amount of material is extruded from the top sheet when exposed to excessive shoulder penetration, resulting in excessive top sheet thinning, creating upward bending, and gap formation between the sheets [118,119]. Therefore, 0.2 mm shoulder penetration is generally applied in conventional FSSW [120,121].

In conventional FSSW, heat generation by the shoulder of the tool is somehow low unless a dwell period is used. During the dwell period, shoulder contribution in the generation of heat and flow of material is significantly enhanced such that the highest fraction of energy generation takes place during this period [109]. Nasir *et al.* [122] studied the effect of welding parameters (rotational speed (RS) and dwell time) on the microstructure and mechanical performance of dissimilar AA5754 and AA7075-T651 by FSSW. RS and dwell time vary in the ranges of 1,000–1,400 rpm, and 2–5 s, respectively. The maximum tensile shear force was 806.3 N at 1,000 rpm and 2 s dwell time. The material becomes soft at 1,400 rpm compared to a lower speed of 1,000 rpm. In addition, dissimilar inter-mixing does not take place in spot welds formed by a threaded tool with no dwell period. The reason for getting high strength at low RS and dwell time is the generation of low heat input. While high RS and high dwell time lead to high heat input which causes a raise in the grain size that

decreases the joint strength [97,123]. Moreover, the addition of dwell periods extends the spot welding cycle which could be an important issue when the completion time of the target weld has to be less than or equal to that of resistance spot welding (RSW). In pinless FW, a much greater direct contact area is made between the material and shoulder, enhancing the flow of the material and significantly increasing the temperature when applying a short dwell time [124,125]. Such fast welding cycles (<1 s) cause less HAZ softening in heat-treatable Al alloys [126–128]. The mechanism of heat generation during FSSW differs from that in linear FSW because FSSW is a very transient joining process [129]. In pinless FSSW, generally a shoulder with a diameter of 10 mm is applied [130–132].

The results obtained from numerical simulations reveal that sleeves with greater outer diameters greatly increase the flow velocity, heat input, and welding spot area where a sleeve of 9.0 mm in diameter was most commonly applied in RFSSW [133–138]. In the comparison between adhesion bonding joints and FSSW, the results show that there is no significant use of adhesions instead of FSSW, also the mechanical performance of FSSW was higher than adhesive joint [139,140]. Goushegir *et al.* [105] studied the process parameters on mechanical performance and bonding area of aluminum Carbon fiber-polyphenylene sulfide (CF-PPS) and Al alloy AA2024-T3 with rotating speed of 1,900–2,900 rpm. Plunge depth (PD) was in the range of 0.5–0.8 mm and the obtained results revealed that tool PD significantly affected lap shear force. The PD of the tool into the Al is also statistically significant when analyzing ultimate lap shear force ULSF as the response. The PD influences the shape of the metallic nub and therefore thermo-mechanical interlocking takes place between the Al and the composite. The formation of the metallic nub and its insertion into the composite leads to the increased macro-mechanical interlocking and strength of the joints, especially under shear loading as shown in Figure 5.
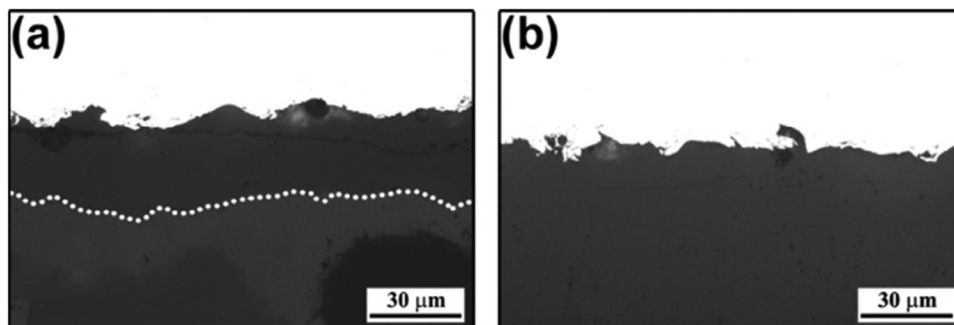

Figure 5: (a) and (b) shows the cross-sectional images of the joints inside the plastically deformed zone with RS of 2,900 rpm and joining pressure 0.2 and 0.3 MPa, respectively [105].

A larger metallic nub increases the macro-mechanical interlocking. Joining time is also an important parameter; when time is short, the molten PPS has low viscosity, therefore to enhance the flow of molten PPS, a high PD and lap shear force varying in the range of 1,698–2,310 N are required. Increasing RS, PD, and joining pressure (JP) increases the lap shear force, whereas increasing the joining time reduces the lap shear force. The comparison between the influence of process parameters on the responses shows that RS and JP significantly influence both the plastically deformed zone area and the lap shear force. During the process of FW, temperature varies in the range of 370–474°C. The temperature in each condition was high enough to allow the deformation of Al under the tool and the formation of the metallic nub. The rate of cooling and heating in this study were 17 and 97°C/s, respectively, which is very fast. Andre et al. [141] investigated the effects of rotating speed and joining pressure on the mechanical strength and microstructure of friction spot welding of CFRP and Al alloy AA2024-T3 with 100 μm PPS film interlayer. JP and RS vary in the ranges of 0.2–0.3 MPa and 1,900–2,900 rpm, respectively. They reported that lap shear force increased from 2,700 to 3,070 N, which was higher than those for joints without interlayers because of their improved micromechanical interlocking, better load distribution, and larger bonding area. Furthermore, compared to the joints without an interlayer, an increase in ultimate lap shear force by 55% was observed in this work for the joints with additional interlayer produced with low heat input conditions. In the case of the high heat input condition, an average improvement of 20% was reached. The temperature was measured on the top surface of a work piece, temperature varies in the range from 325 to 417°C. In the microstructure of interfaces, two bondings were found, the PPS into the crevices of Al and CFRP entrapment by Al deformed as shown in Figure 6. Furthermore, the peak temperatures were above the melting point of the PPS matrix of the CF-PPS and the PPS film (T_m = 280°C). Therefore, the PPS film and a thin layer of the PPS matrix of the CF-PPS composite were melted and recrystallized during the friction stir joint process.

Goushegir et al. [142] applied Al alloy A2024-T3 and carbon fiber poly(phenylene sulfide) CF-PPS as test specimens, presented friction spot welding of single lap joint,
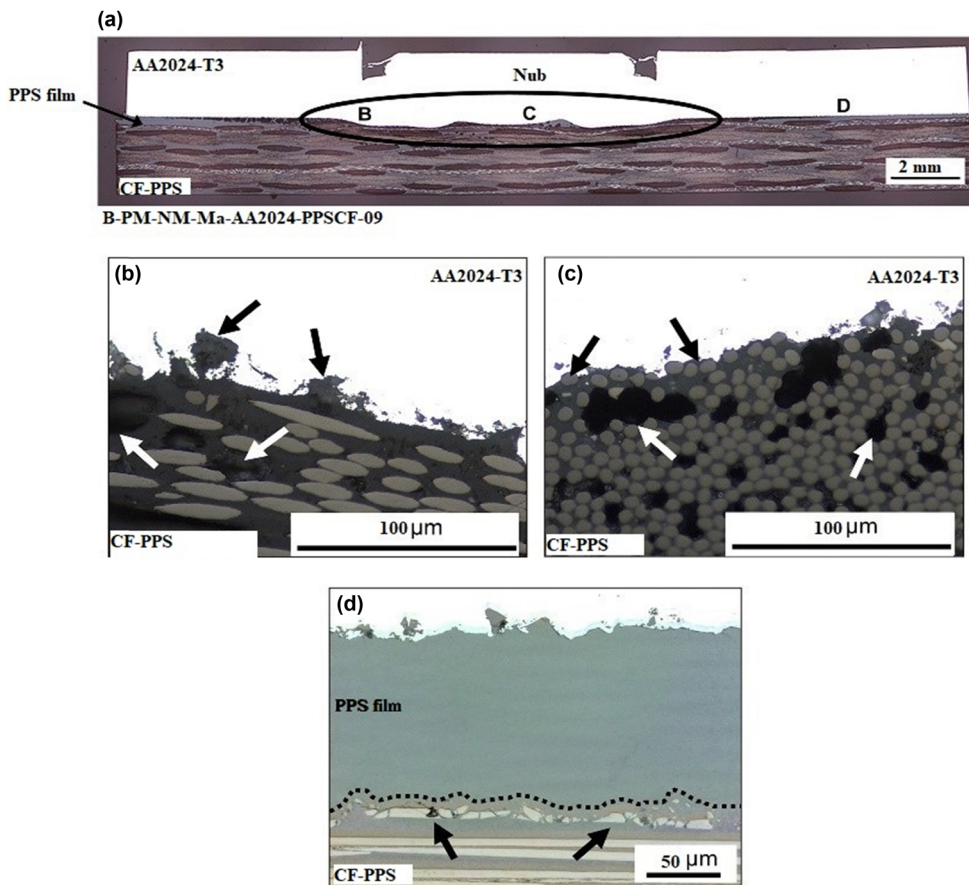

Figure 6: Microstructural details of joint: (a) cross-section with interlayer, (b) molten polymer of Al surface, (c) deformed aluminum, and (d) interface of Al/interlayer [141].

and evaluated the obtained joint results based on their microstructure and mechanical performance. In this study, PD and joining time were fixed at 0.5 mm and 4.8 s, respectively. RS was increased from 1,900–2,900 rpm. The highest rotation speed obtained for the optimum value of shear force was around 1,254 N. Increase in joining area resulted in more intimate contact between PPS matrix and CFRP with Al and hence better mechanical performance. This also increased tool PD and joining time. The influence of increasing PD on lap shear force and displacement at the peak load of joints (762.6 ± 182.7 N/0.45 ± 0.08 mm for PD of 0.5 mm and 1,276 ± 181.5 N/0.65 ± 0.05 mm for PD of 0.8 mm). This trend is associated with the generation of a more pronounced "nub" and increased intimate contact at the composite/Al interface, which can increase adhesion forces by micromechanical interlocking. Joining time and RS increase heat generation and change microstructure and lap shear strength, while intermediate RS and longer joining time lead to greater consolidated polymeric layers at the metal/composite interface. Molten PPS matrix fills these pores/crevices, which, after consolidation, increases the micro-mechanical interlocking and global shear strength of the joint. Another important phenomenon is also observed: a portion of CFRP is entrapped by plasticized Al, thereby creating a micro-mechanical interlocking. Esteves *et al.* [102] studied the effects of different parameters on the mechanical strength and microstructure of CF-PPS and Al alloy AA6181-T4 joined by friction spot welding. In this study, the rotating speed was increased from 1,200 to 1,600 rpm. The maximum shear force was 3,523 N with a RS of 1,200 rpm, PD of 1.15 mm, and joining time of 6 s. Higher heat input induces the formation of large bonded areas, as visually confirmed by a large amount of PPS molten layer at the interface. This can be seen in fracture surfaces. Moreover, pronounced nub formation was observed due to the large heat input. Increase in joining time and rotating speed directly increased heat generation and changed lap shear strength and microstructure. Heat input is responsible for PPS molten layer in the joint interface increasing the bonding area. Moreover, PD plays an important role in macro-mechanical interlocking mechanisms at the metal/composite interface controlling the formation of the metallic nub. The higher the PD the more pronounced the metallic nub will be, as shown in Figure 7.

Andre *et al.* [143] evaluated the mechanical performance of Al alloy AA7075-T6 and CFRP by FSSW. In this study, rotating speed, joining time, and PD were 1,900 rpm, 4 s, and 0.8 mm, respectively, and joining force was varied from 4 to 8 kN. The obtained result showed that lap shear force was 4,068 N and joining force significantly affected nub geometry at 6 kN. It is worth noting that, for all the investigated joints, a layer of the reconsolidated molten
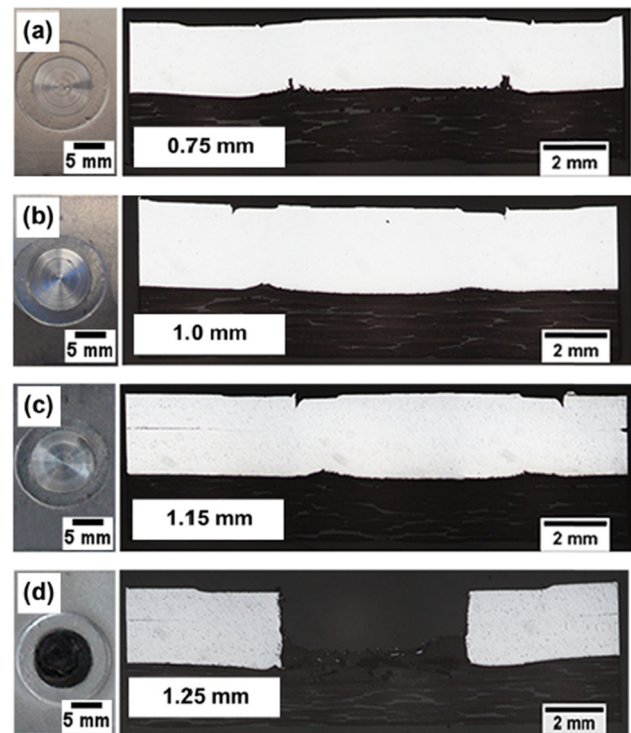

Figure 7: Cross section micrographs from top and mid views in different plunge depths: (a) 0.75 mm, (b) 1.0 mm, (c) 1.15 mm, and (d) 1.25 mm [102].

PPS was formed and remained attached to the Al surface providing adhesion forces. Additionally, signs of fiber and matrix entrapment on the Al surface were observed in all cases. It is possible to note that an effective micro-mechanical interlocking was achieved because PPS matrix took the shape of the irregularities of the Al surface, while some fibers were entrapped into crevices. The maximum temperature on the Al surface was 331°C. The bonding area was divided into various zones, namely adhesion zone (AZ), transition zone (TZ), and plastically deformed zone (PDZ), as shown in Figure 8. These zones were formed during the welding process and air bubbles were formed when the molten matrix moved from the center to the edge of the joint.

Andre *et al.* [107] studied the mechanical performance and microstructure of CFRP and Al alloy AA2024-T3 joints formed by FSSW with an additional PPS film interlayer. Rotating speed was varied from 1,300 to 2,500 rpm. The optimal tensile shear force of about 2,000 N was obtained at 1,900 rpm rotating speed, 0.8 mm PD, and 6 s joining time, and showed linear elasticity before the final catastrophic failure. The PD of the sleeve is also a very important process parameter because it is directly related to nub formation and its final geometry, mechanical interlocking between the joining partners and consequently to the joint
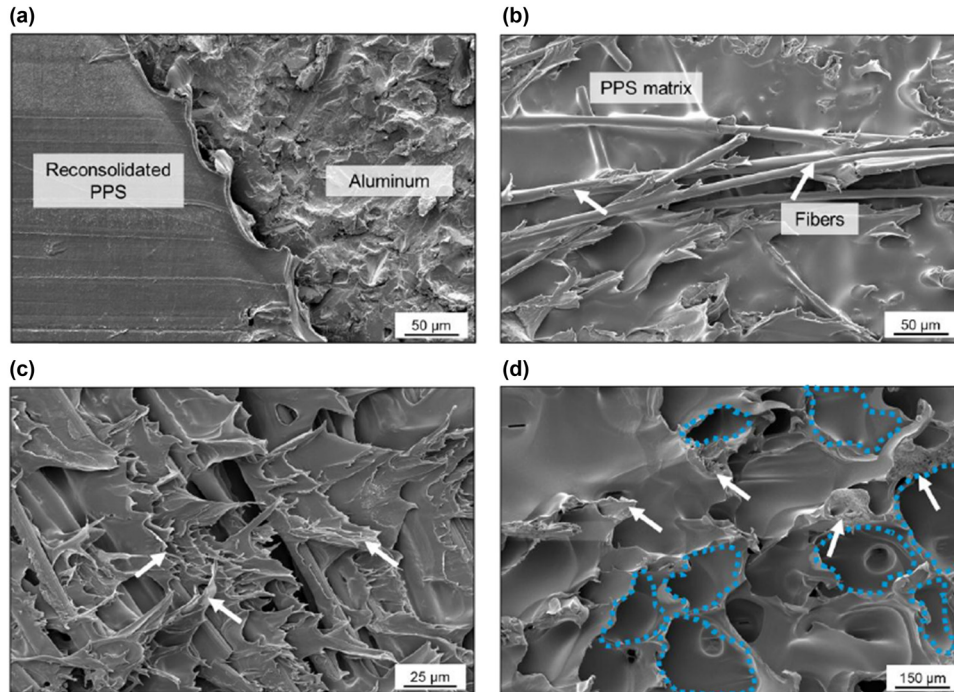
Figure 8: SEM image: (a) transition between AZ and TZ, (b) PDZ of Al surface, (c) PDZ, and (d) TZ on the composite surface [143].

strength. A high RS of 2,500 rpm resulted in an accentuated decrease in molten viscosity supporting the squeezing of the molten interlayer outside the metallic nub area. The area around the nub cohesive failure dominates the polymer matrix and the remaining CFRP will be attached to the Al. In this study, the influence parameters show the effect of PD on the lap shear force. Manente André *et al.* [144] improved the adhesion mechanisms and mechanical performance of Al alloy AA2024-T3 and CFRP with additional 100 μm PPS film interlayer FSW. In this study, RS, PD, and joining time were 1,900 rpm, 0.8 mm, and 4 s, respectively. The optimal tensile shear force was 3,068 N obtained at a high roughness effect on contact surface area. Also, sandblasting was found to be the most effective treatment which maximized the performance of mechanical joint. Increase in roughness creates crevices on the surface and enlarges effective contact area, contributing to micro-mechanical interlocking and establishing adhesion forces. Impressions containing pieces of CFRP removed from PPS matrix were identified on interlayer fracture surface after lap shear testing. This is an indication of an effective micro-mechanical interlocking at the interface of interlayer composite achieved with sandblasted specimens.

Andre *et al.* [145] studied the influence of PPS film interlayers with different thicknesses on the mechanical performance and microstructure of Al alloy AA2024-T3 and carbon fiber CF-PPS by friction spot welding. In this work, rotating speed, PD, and joining time were 1,900 rpm, 0.8 mm, and 4 s, respectively, and 2 different interlayer thicknesses of 100 and 500 μm were investigated. The results showed that the maximum temperature was 360°C in both cases. The volume of metal deformation was embedded slightly in CFRP during welding with 100 μm interlayer. On the other hand, with a 500 μm interlayer, the formation of the metallic nub arises through the embedding of the deformed metal in the interlayer film, without reaching the composite. Also, bubbles were trapped in polymer and resulted in the creation of cavities after the solidification of the welding joint. Maximum shear forces were 2,093 and 708 N in the case of 100 and 500 μm interlayers, respectively. The thinner 100 μm film was softened more efficiently than the thicker 500 μm film by the frictional heat generated during the joining process. Accordingly, although the Al/film interface had effective micro-anchoring for both joints, film/composite interface displayed greater cohesion for the joints with 100 μm thick film. More efficient softening of this interlayer film favors inter diffusion of the PPS chains of the matrix of composite and film. The film with lower thickness presented better results than the higher thickness interlayer.

Ogawa *et al.* [146] studied the effects of welding properties of FSSW of Al alloy AA5182 and CFRP. Tool rotating speed was 3,000 rpm and welding time was set to 1, 2, and 5 s. The results showed that temperature on Al

surface varied from 200 to 250°C. Also, average static strength for 1, 2, and 5 s welding times were 4.1, 5.5, and 7.1 kN, respectively. Static strength was significantly improved by increasing welding time. Microstructural results showed that pores were formed on CFRP side which mainly concentrated under the tool center. Resin-based CFRP was melted just under tool periphery and a layer of resin was preserved between the two materials. As it has been observed that with increase in the dwell time, the joint strength increases due to the high heat input which increases the joint area and melts the resin as well. Goushegir [12] studied friction spot welding of CF-PPS and Al alloy AA2024-T3. Rotating speed, PD, and joining time were 2,900 rpm, 0.8 mm, and 4 s, respectively. The obtained results showed that temperature varied between 345 and 474°C. The temperature of approximately 400°C lies in the range of dynamic re-crystallization of AA2024 for friction-based joining processes. Microstructural zones were divided into different areas: polymer heat affected zone (PHAZ), heat affect zone (HAZ), thermo-mechanical affect zone (TMAZ), and stir zone (SZ). Different microhardness values were observed in different zones; in the base material (zone 1) average hardness was 135 HV, in the string zone, high microhardness of 151 HV was observed, the average hardness of TMAZ was 139 HV, and the lowest

microhardness of 123 HV was witnessed in HAZ. Also, the average ultimate lap shear force was 8,264 N, while reference bonded was shown to be 5,459 N. This was explained by the fact that the primer was a carbon-based epoxy layer leading to the formation of very strong carbon–carbon primary bonds with PPS consolidated layer during joining cycle.

Ogawa *et al.* [147] studied FSSW of CFRP and Al alloy AA5182. The rotating speed was 3,000 rpm. It was confirmed that pores were present inside CFRP, irrespective of the treatment of the surface in the microstructure of the welding joint. These pores were assumed to be developed either by the air entrapped by molten resin flow or during CFRP molding which was then expanded because of frictional heat. The average static strengths of the untreated, porous layer and organic coating series were approximately 5.7, 6.6, and 7.4 kN, respectively. Hence, surface treatment was found to enhance FSSW joint static strength. The shoulder diameter was 10 mm and the probe length was 0.35 mm. Amancio-Filho *et al.* [148] studied the FSSW of magnesium AZ31 and carbon fiber-reinforced polymer. In their research, rotating speed was varied from 900 to 3,000 rpm, PD was in the range of 0.25–1.75 mm, and joining time was changed from 3 to 8 s. The results showed that on PPS-CF/AZ31 surface, the temperature was varied in
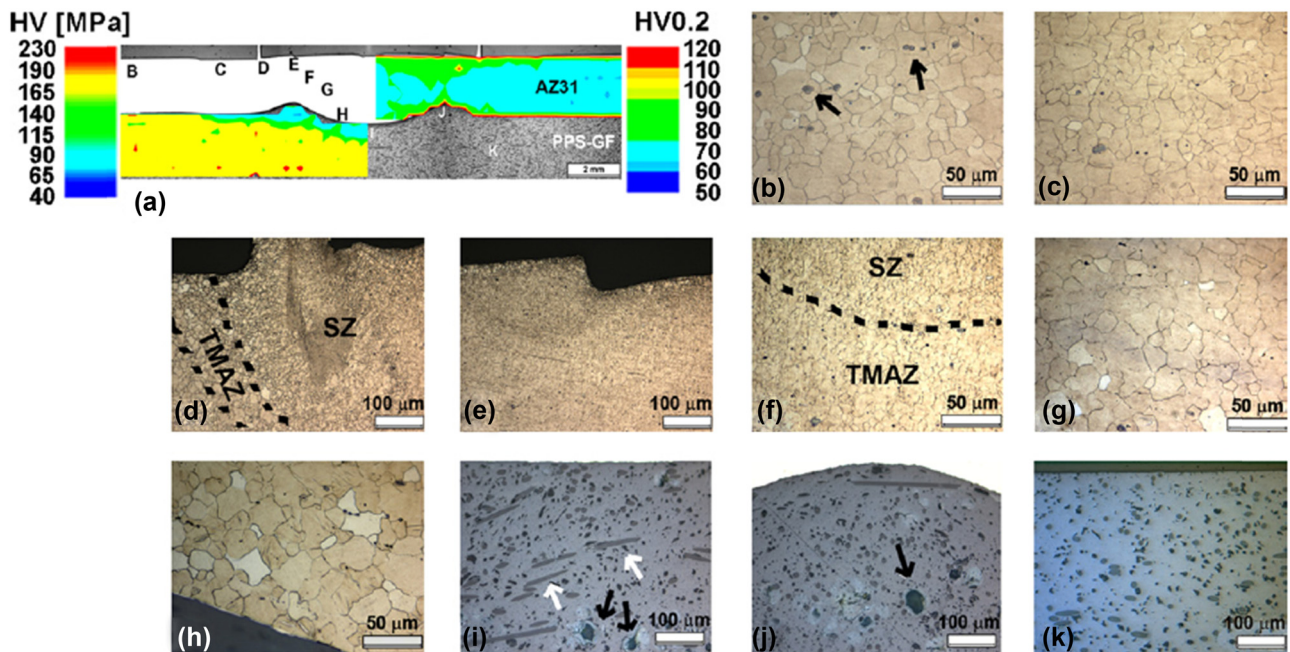

Figure 9: : Hardness and microstructure of AZ31 joint: (a) cross-section image pf microhardness and macrograph maps; (b) AZ31 base material upper region; (c) AZ31 volume below clamping ring; (d) transition details between SZ and TMAZ; (e) SZ center; (f) transition region of TMAZ and SZ; (g) heat affected zone central region; (h) polymer–metal interface within metallic nub; (i) consolidated polymer layer underneath metallic nub; (j) consolidated polymer layer close to metal–polymer interface, and (k) the upper portion of base material polymeric plate [148].

the range of 400–440°C (1,500 rpm, 0.25 mm, and 8 s). SZ was characterized by fine dynamic recrystallized grains. In microstructure, the SZ showed that $Mg_{17}Al_{12}$ dispersed particles and could be observed. Although the bonding mechanisms of joint are not yet well understood, there are strong indications that joining is accomplished by a mixed regime of surface mechanical interlocking and adhesion between the metallic and consolidated polymeric layers, as well as direct partial fiber attachment on the metallic plate. A thin transition zone between the HAZ and SZ is called the TMAZ, as illustrated in Figure 9. Tensile shear force was 2,000 N in AZ31/PPS-GF but only 1,500 N in AZ31/PPS-CF.

Goncalves *et al.* [149] studied FSSW of polyamide 66 laminate reinforced with CFRP. During the welding, the plunge was a depth of 2 mm and the rotation speed was 3,000 rpm. According to these parameters, the average strength of lap shear was 26.8 MPa from a nominal area of 63.6 mm^2 in the external diameter of the sleeve. Mechanical and thermal effects were evident in the material around the sleeve. However, in their early stage of development, these welds showed comparable mechanical performance to similar joints produced with state-of-the-art welding technology reported in the literature. This region was called the SZ, as shown in Figure 10, which was mixed between polymer and broken CFRP.

Huang *et al.* [150] studied carbon fiber polyetherimide laminate friction spot welding. In this study, PD was 2.2 mm, dwell time was 2 s, and rotating speed varied from 800 to 1,200 rpm. Welding tool was made of titanium alloy to reduce heat loss, which consisted of a clamping ring, sleeve, and pin. At low rotating speeds, thermoplastic materials cannot be softened completely. With the increase in the rotating speed, defects are reduced and appeared only at the border of the sleeve. Thickness reduction or unfelling defect appeared at the pin refilling zone (PRZ) on the joint surface. The microstructure in this joint was divided into a sleeve stirring zone (SSZ) and a thermo-mechanically affected zone. CFRP and polyetherimide laminate showed long circular fibers because of the stacking sequence. Meanwhile, the lower thermal conductivity of the polymer is difficult to make frictional heat conduct to the middle interface between the upper and lower sheets, and then the lack of adhesive joining forms. The length of no adhesive joining area was gradually decreased with the increase in the rotational velocity due to the improvement of thermo-mechanical behavior. Also, the maximum and minimum tensile shear forces were about 1,600 and 1,250 N at rotating speeds of 1,200 and 800 rpm, respectively. With increase in the rotational velocity to 1,000 rpm, the improvement of effective joining length benefited from joint strength compared with the rotational velocity of 800 rpm.

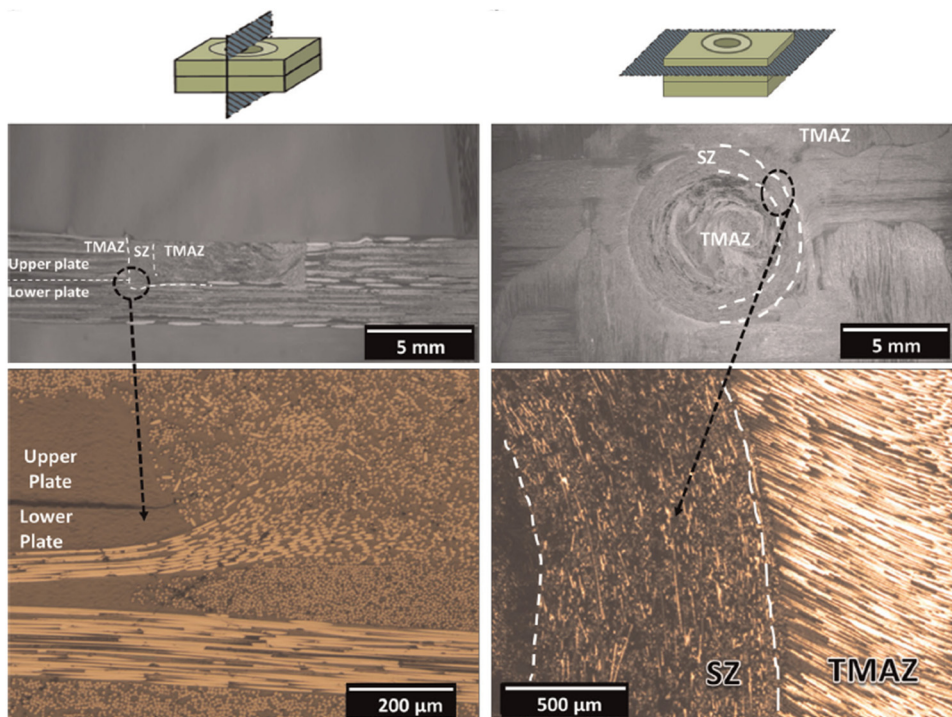Goncalves *et al.* [151] studied the improvement of FW joining polyamide 6 and polyamide 66/carbon fiber

Figure 10: CF-PA66 weld microstructure produced by FSSW [149].

laminate. There were two conditions in this work. Rotation speed and depth of penetration were fixed at 1,500 rpm and 3.8 mm, as conditions A and B, respectively. The diameter of clamping was 14.5 mm in condition A and 22 mm in condition B. The results showed that maximum temperatures were 280 and 352°C, respectively. Microstructure cross-section in condition A had a depth of 3.08 mm, while in condition B it was only 0.74 mm. The corresponding tensile shear forces were 1,323 and 2,196 N in condition B. The welding of thermoplastics by FW required larger thermal inputs during welding compared to metals, owing to the low thermal conductivity of polymers. If the larger thermal input of condition B was used with tool geometry optimized for welding metals, the tool would penetrate all the way through the specimen, making welding impossible. Bolouri *et al.* [152] studied a new design of joining Al alloy Al 1050 and CFRP with 50% fiber with FSSW. Rotating speed was varied in the range of 2,500–3,000 rpm and joining time and dwell time were 4 and 2 s, respectively. PDs were in the range of 0.8–1.0 mm and the average temperature was increased from 310 to 400°C by increasing the rotating speed from 2,500 to 3,000 rpm. Changes in the feed rate and PD of the pin affect the joining temperature. The joint between Al and CFRP was unsuccessful at PD of 0.75 mm. An increase in PD to 1.25 mm resulted in a successful joint. Also, an increase in PD from 1.25 to 1.30 mm enhanced lap shear strength from 230 to 241 N. Interlocking between Al and CFRP increased the performance of the joint and shear force showed brittle fracture in the joint. The hooks noticeably retained the CFRP attached with Al alloys, which increased the strength of joints. In addition, as a result of the creation of more pronounced nub and hooks, the intimate contact at the interface of Al alloy and CFRP was increased that could further push the molten resin to fill into the crevices on the surface of Al alloy.

Nasir *et al.* [153] successfully conducted experimental studies on CFRP as an interlayer in dissimilar AA7075-T651 and Ti-6A-4V alloys by FSSW at specified welding parameters (RS and dwell time) and investigated the mechanical and microstructural properties of welded joints. The obtained results showed that the mechanical performance of the weld joint was increased with the increase in RS. A maximum tensile shear load of 2,597.8 N was gained at a RS of 2,000 rpm and a high dwell time of 10 s. Dwell time had a significant effect on the mechanical properties and raised tensile shear load to 54.7% at a high RS. The hardness of the weld joint was increased by RS and 18.90% improvement was observed in the keyhole of a weld joint. One thing that has been noted with joints made with CFRP interlayer was that they had low tensile strength compared to metals without interlayer. On the other hand, at high RS

and high dwell times without CFRP interlayer, low tensile strength was observed which was resolved in the case of CFRP interlayer with dissimilar metal alloys. Kalaf *et al.* [154] applied CFRP as an interlayer in similar Al alloy AA5052 to investigate the effects of welding parameters (RS and dwell time) on the mechanical properties, joint efficiency, and microstructure of the friction stir spot weld joint. The maximum tensile shear load of 1,779.6 N was obtained at 2,000 rpm and 2 s. A significant improvement in hardness (29%) was obtained in the key whole area at high RSs and high dwell times. The best tensile shear load was 7.1 kN obtained for AA5182 and CFRP by FSSW at RS of 3,000 rpm and welding time of 5 s; the thickness for AA5182 and CFRP were 1.2 and 3 mm, respectively. The joints were improved as the welding time was increased. This grain was affected by a larger welding area and increased resin melting. So, increasing welding time was effective in improving the joint strength.

4 RFSSW of CFRP

Researchers at Helmholtz-Zentrum Geesthacht (Germany) introduced and patented RFSSW in 1999 for joining two or more sheets made of lightweight materials like Al and Mg alloys [155]. Joint was prepared by plasticization and material displacement in a process similar to back extrusion. The most important advantage of RFSSW is the lack of keyhole structure in the weld where the weld is nominally flush with the original surface. According to Figure 11, the tool applied in RFSSW comprises an inner pin, a sleeve, and an outer stationary clamp ring. The clamping ring firmly held work pieces in contact throughout the welding and prevented the sheets from separating and lifting when plasticized material was displaced by sleeve and pin [156–159].

Using one single motor, the pin and sleeve rotated at the same speed and along the same direction and were independently moved up and down by separate actuators. RFSSW process is more complicated than conventional FSSW and, depending on the plunging component, could be classified into sleeve plunge and pin plunge variants. A schematic diagram of the sleeve plunge variant is shown in Figure 11. First, the sleeve was plunged into the work piece to a previously calculated depth for material plasticization, while pin moved upward to form an accurate cylindrical cavity for the accommodation of the plasticized material squeezing out by sleeve. Once a certain dwell time was passed, pin and rotating sleeve returned to their original locations and extruded the
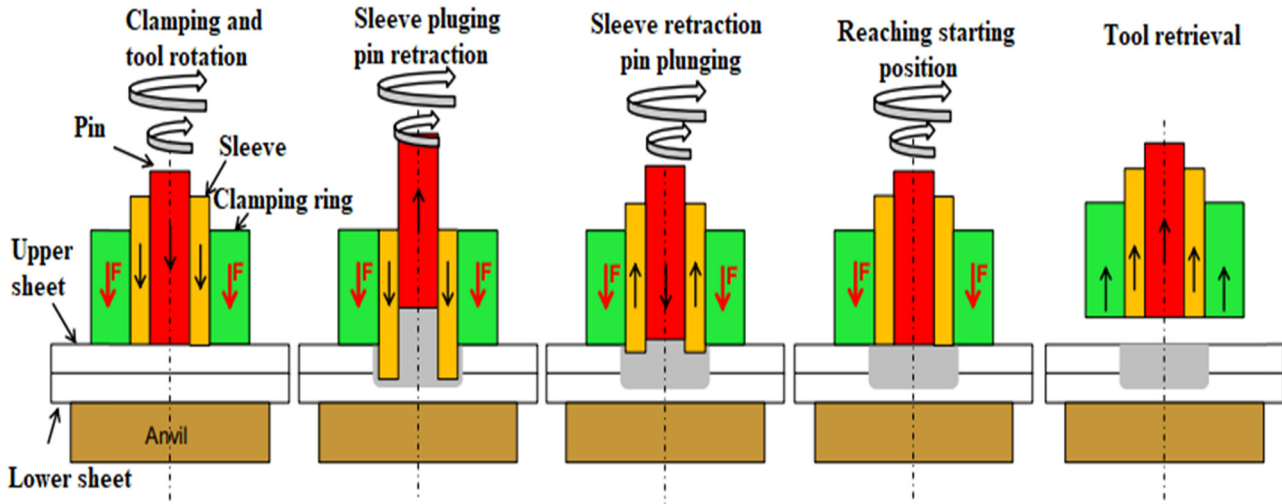
Figure 11: Schematic diagram of RFSSW [164].

softened materials into the joint creating a spot weld with zero or minimum surface indentation. The key advantage of sleeve plunge variant over pin plunge variant was its highly strong weld because of greater nugget size. However, this variant demanded higher plunge forces [157,160–163].

The refill method achieves overlap shear strength that compares favorably to self-piercing riveting, RSW, and conventional FSSW, with joining times almost similar to the latter [95,165]. Also, RFSSW has some advantages such as the ability to join lightweight materials including polymers and Mg and Al alloys [166] and dissimilar pairs such as polymers to metals [148] and ferrous metals [167–169] to non-ferrous metals [170,171]. RFSSW has been successfully applied in the fabrication of skin stiffened panels [172], filling of keyholes resulting from FSSW, rivet or fastener replacement, RSW replacement, repairing fatigue cracks, and as a tacking welding method for FSSW [173–175].

In RFSSW, the depth of plunge is more flexible and is defined as the PD of plunging element (either pin or sleeve). Pin lengths which do not reach bottom sheet, decrease the strength of spot weld tensile because the keyhole formed by pin decreases the cross section. When tool pin is penetrated into bottom sheet, it contributes to bond formation providing mechanical strength. At the RS of 2,000 rpm, the numerically obtained velocity field of the material just under tool pin is about 50% of that beneath the shoulder. It is noteworthy that the bottom of the pin has a certain distance from the bottom of the shoulder and therefore its contribution is remarkably enhanced. With the increase in pin length, its role in the total velocity field is increased. At a critical length, pin increases weld zone size and improves weld joint strength [176]. At pin lengths

beyond the material flow zone formed by the shoulder, strength could be decreased because of excessive plunging resulting in the extrusion of a portion of the bottom sheet significantly decreasing the thickness of the bottom sheet under the pin [162,177–179].

Threads in RFSSW are generally machined on pin and sleeve to decrease the contamination of interfaces among three tool components [180]. Ji *et al.* [181] applied a 3D finite element model to study grooved sleeve effects on the flow of materials and concluded that grooved sleeves increased the velocity of material flow, and grooves on the inner walls of sleeves outperformed those with lower widths on the outer walls of sleeves. Scrolled grooves were more favorable than concentric circular grooves at the bottom of sleeves in decreasing the thickness of bonding ligament and increasing the area of bonding. Pabandi *et al.* [182] studied RFSSW of Al alloy AA5252 with short carbon fiber polypropylene (PP-SCF) and applied 500–2,000 rpm rotating speed and 5 s dwell time. A cylindrical tool from heat-treated H13 steel composed of a shoulder with a diameter of 20 mm was employed as the welding tool. They found that the optimal shear tensile was 350 N at 2,000 rpm and the maximum hardness was 68 HV obtained at 500 rpm, as shown in Figure 12. Temperature evaluation was performed at various distances from the center of the joint and the maximum value was found to be 340°C, 10 mm from the joint center. Scanning electron microscope (SEM) images showed 15 μm at the interface reaction layer and it seemed that the layer was formed by an erosion mechanism. Also, a reaction layer was created between Al and molten polymer and was re-solidified inside the hole, as illustrated in Figure 13.

Ashong *et al.* [183] studied the RFSSW of dissimilar CFRP and AA6014 alloy. The Joint was created at
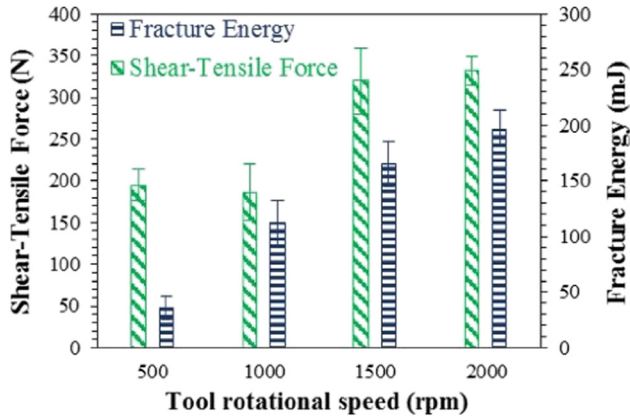
Figure 12: Shear tensile force and fracture energy at different rotating speeds [182].

1,000 rpm rotating speed, 1.5 s joining time, and 1.9 mm PD. The results showed that the average tensile shear force was 1.63 kN and joint efficiency was 10%. Microscopy of CFRP and Al showed tight bonding on the interface of the joint with no visible defects. The current work compared the obtained results with those of other joints after surface treatment and found that refill friction spot welding was a suitable method for manufacturing metal-polymer hybrid production. Micro mechanical and chemical interlocking were the main influencing factors in tensile shear force.

Regarding the review on RFSSW, the best tensile shear load was 1.63 kN which was obtained for AA6014 and CFRP at a RS of 1,000 rpm and joining time of 1.5 s, the thickness for both AA6014 and CFRP was 2 mm. Macroscopic images of the tensile shear fracture surfaces showed that both interfacial and base-plastic fractures occurred in the joint. The average tensile shear strength and efficiency of the joints were 26 MPa and 10%, respectively. The summary of research works on FSSW, RFSSW, and CFRP are summarized and presented in Table 1.

5 FSW of CFRP

This section describes the FSW technique in more detail, since the main goal of this work was to investigate this technique. The Welding Institute first introduced FSW in 1991 in UK [185–189]. As discussed in Section 1, FSW was first developed for welding similar materials, such as AAs and other light alloys [190–192], but it can also be applied for joining dissimilar materials [6,193]. This method has been applied in a wide variety of industries such as automotive, aerospace, and maritime industries [194,195]. In the aerospace industry, this method could be employed in producing thin alloy skins, fuel tanks, and airframes [196], and all major European manufacturers of airframe and some research institutes address FSW problems [197,198].
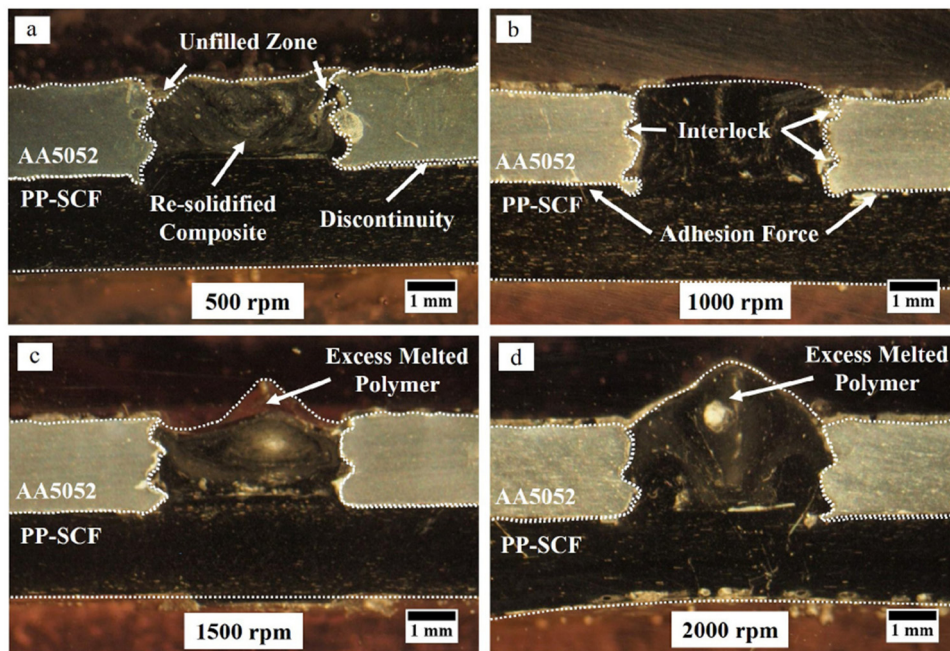

Figure 13: Cross-sectional view at different rotating speeds (a) 500 rpm, (b) 1,000 rpm, (c) 1,500 rpm, and (d) 2,000 rpm [182].

Table 1: Summary of research works performed on FSSW and RFSSW of carbon fiber-reinforced polymer with materials

No.	Material type & thickness in (mm)	Type of welding	Parameters					Temperature (°C)	Tensile shear force (N)	Type of joint	Ref.
			Rotational speed (rpm)	Joining time (s)	Plunge depth (mm)	Joining pressure (MPa)	Dwell time (s)				
1	Carbon fiber/2	AA5052/2	RFSSW	500 1,000 1,500 2,000	—	—	—	5	190 230 270 340	190 180 320 350	Single joint	[182]
2	Carbon fiber/2.17	AA2024-T3/2	FSSW	1,900 2,400 2,900	4 6 8	0.5 0.65 0.8	0.2 0.25 0.3	—	≈420 445 ≈474	1,930 2,080 2,230	Single joint	[105]
3	Carbon fiber/2.17	AA2024-T3/2	FSSW	1,900 2,900	4 4	0.8 0.8	0.2 0.3	— —	325 417	2,700 3,070	Interlayer 100 µm	[141]
4	Carbon fiber/8 Carbon fiber/2.1	AZ31m/12	FSSW	900–3,000 900–3,000	3–8 4–8	0.25–1.75 0.25–0.35	2–3 2.4–3	—	400–440	1,500 2,000	Single joint	[148]
5	Carbon fiber/2.17	AA2024-T3/2	FSSW	1,900 2,900	4–8 4–8	0.5 0.5	— —	—	350 400	950.6 1,254	Single joint	[142]
6	Carbon fiber/2.17	AA6181-T4/1,1.5	FSSW	1,200 1,400 1,600	1 4 7.5	0.75 1 1.15	1.15 6 8.3	— — —	— — —	2,107–3,523 3,241–3,254 3,153–3,248	Single joint	[102]
7	Carbon fiber/2.17	AA7075-T6/2	FSSW	1,900	4	0.8	—	—	331	2,500	Single joint	[143]
8	Carbon fiber/2.17	AA2024-T3/2	FSSW	1,900	6	0.8	0.3	—	400	2,000	Interlayer 100 µm	[107]
9	Carbon fiber/2.17	AA2024-T3/2	FSSW	2,900	4	0.8	0.3	—	—	—	Single joint	[184]
10	Carbon fiber/2.17	AA2024-T3/2	FSSW	1,900	4	0.8	0.2	—	110	3,068	Interlayer 100 µm	[144]
11	Carbon fiber/2	Polyamide 66 and 2	FSSW	3,000	7.5	2	12 kN	—	266	—	Single joint	[149]
12	Carbon fiber/2	Polyamide 66 laminate and 4	FSSW	1,500 1,500	— —	— —	— —	2 8	280 352	1,323 2,196	Single joint	[151]
13	Carbon fiber/2	AA6014/2	RFSSW	1,000	1.5	1.9	—	—	—	1,630	Single joint	[183]
14	Carbon fiber/2	AA1050/2	FSSW	2,500–3,000	4	0.8	—	2	310–400	230–241	Single joint	[152]
15	Carbon fiber/2	PEI laminate	FSSW	800–1,000–1,200	—	2.2	—	2	—	Max 1,600	Single joint	[150]

(Continued)

Table 1: *Continued*

No.	Material type & thickness in (mm)	Type of welding	Parameters					Temperature (°C)	Tensile shear force (N)	Type of joint	Ref.
			Rotational speed (rpm)	Joining time (s)	Plunge depth (mm)	Joining pressure (MPa)	Dwell time (s)				
16	AA2024-T3/2 Carbon fiber 2.17	FSSW	2,900	4	0.8	0.3	—	345–474	5,459–8,264	Single joint	[12]
17	AA2024-T3/2 Carbon fiber/2.17	FSSW	1,900	4	0.8	0.3	—	360	2,093–708	Interlayer 100–500 µm	[145]
18	AA5182/1.2 Carbon fiber/3	FSSW	3,000	1,2,5	1	—	—	200–250	4100,5500,7100	Single joint	[146]

In this approach, a cylindrical tool containing a profiled pin is plunged into the joining areas of components and rotated at an accurate RS. This creates plastic deformation in the joining area due to stirring and heating. Therefore, the material is softened and mixed. With the progress of the tool, the joint is cooled and consolidated [199,200]. It should be noted that tool material has to be more resistant than components to be welded [201]. A schematic diagram of the technique is depicted in Figure 14.

Key technical parameters included feed rate, shoulder penetration, applied force, rotational speed, and tool geometry [202–206]. Tool geometry refers to pin shape (tapered or simply cylindrical) and the diameters of pin and tool [207]. The key advantage of FSW is that it does not need to reach component melting points. Therefore, the developed residual distortions and stresses are significantly lower than other common welding methods [208–211]. It also has other advantages including non-consumable tool nature, joint resistance to corrosion, and no need for filler materials. The most important drawback of FSW is that to date, no special equipment has been developed for FSW [212]. The reason for this was that FSW is a novel method and has not been fully investigated yet [213]. The existing methods were not effective in welding some Al alloys (AAs) and therefore, other methods such as FSW were investigated [214–216]. Krasnowski *et al.* [217] studied the effect of the geometry of tool on FSW welding of Al 6082. Among the three tool types which were applied, the best results were achieved for conventional and Triflute tools. Figure 15 presents the three different models of tools employed in this work.

In Honda Accord model 2013, stamped steel engine cradle and cast Al were joined using this method [218]. In this particular example, a remarkable innovation was the
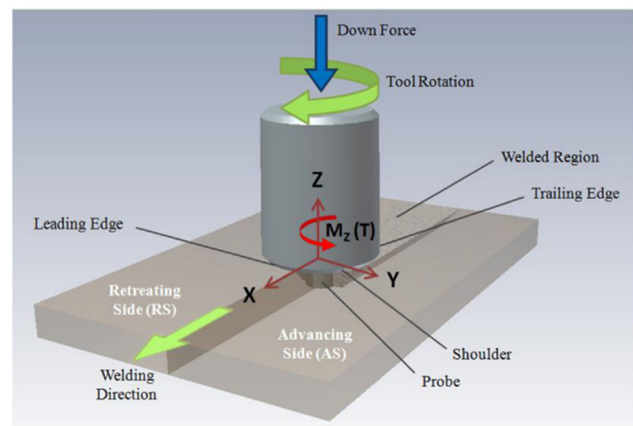

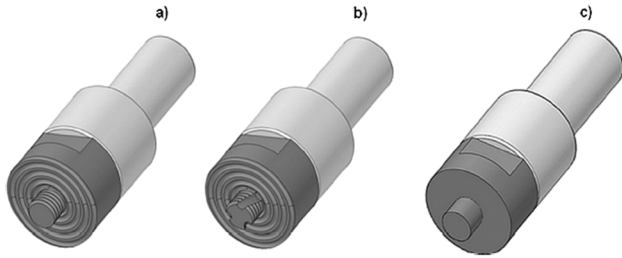**Figure 14:** Schematic diagram of the FW technique [195].

Figure 15: Tool geometries: (a) conventional; (b) triflute; and (c) simple [217].

application of a C-frame linear (FSSW) exerting total axial load on the tool to avoid the necessity of using extremely high load capacity and stiff fixtures and robots for applying axial force on the tool. Another critical point in the method devised by Honda was the application of a sealant to prevent crevice corrosion during field operations. However, limited details are available on the mechanical characteristics of the joints created using this method [219,220]. Haghshenas *et al.* [221] showed that heat-treated H13 steel tool has good resistance to thermal fatigue, erosion, and wear, and is widely used for making molds and dies. It is noteworthy that other works involving adhesive and diffusion bonding have revealed that the decrease in the thickness of intermetallic compound regions or reaction layers increased joint strength [222,223]. Welding parameters remarkably affected energy output (torque and axial force) when welding equipment is under position-control mode. Welding parameters also significantly affected weld temperature [224], heating rate, weld integrity [225], hook geometry, and SZ dimensions of the softened region when an age-strengthened Al alloy sheet was fabricated.

As mentioned earlier, the larger tool shoulder remained in contact with SZ material for almost the entire FSW/FSP operation and therefore, the RS varied in the range of 200–1,000 rpm [226]. Meanwhile, a great fraction of energy was dissipated into joining heat sinks and a limited amount of the energy generated was needed for the formation of SZ which decreased energy efficiency. Hence, the rotation speed of the tool had to be increased to enhance heat input and decrease welding time to make it comparable to RSW and make the axial force of tool compatible with the available welding robot capabilities [227–229]. In pinless FSSW, the depth of shoulder penetration is one of the two critical factors determining the formation and mechanical performance of the weld; tool penetration depth of 0.2 mm is generally applied at a workpiece thickness equal to or above 1 mm [127]. Sometimes, deeper penetration of the shoulder (>0.5 mm) is needed to guarantee sufficient penetration of the deformation zone created by the shoulder into the

bottom sheet when thicker 2 mm sheets are welded [130]. Another key parameter is dwell time which supplies the energy needed for the formation of lower and upper stir zones in sheets [230–232]. In metals with higher melting points, longer dwell times are required for a significant increase in heat input to obtain the temperature needed for plastic flow. On the other hand, it is noteworthy that the width of the softened region created during welding heat-treatable Al alloys is greatly affected by dwell time. In addition, contributions of power input and dwell time are remarkably decreased when a quasi-static state is reached because torque and axial force are remarkably decreased in the dwell period [233,234].

An axial force is applied by the shoulder onto the top surface of the workpiece to create the forging action required for welding consolidation, constrain plasticized material around the pin, and establish frictional heating and deformational material flow in a relatively thin layer under the bottom surface of the shoulder. Plastic flow takes place not only within the stir zone but also in a larger area under the shoulder of the tool [235,236]. It was found that the generation of heat under the large area of the shoulder of the tool was a dominant characteristic in FSW [237–239]. Huang *et al.* [240] studied FSW of Al alloy AA2060-T8 and the tool contained a stationary shoulder, a rotational shoulder, and a tapered thread pin with triple facets. Rotating speed varied from 1,400 to 2,000 rpm and dwell time was in the range of 10–15 s. The results showed that the maximum shear force was 1,550 N for 1,600 rpm, as illustrated in Figure 16. Also, hardness decreased with the increase in the rotating speed, as showed in Figure 17.

At the rotating speed of 1,600 rpm, an increase in the frictional heat improved the plasticized material transfer and eliminated cavity defects. Surface pre-treatments needed to be evaluated for further increase in the strength of interfacial joining between the thermoplastic and material. Also, it is difficult to transfer heat input by tool rotating speed from the top to the bottom plate due to the low thermal conductivity of SCF/PEEK ($0.92\,\mathrm{K\,m^{-1}\,k^{-1}}$), Therefore, partial spin pin only comes into contact with the AA2060-T8 and then produces low friction heat, as a result of a large aluminum anchor. Das and Bang [241] performed numerical and experimental tests on the joining of Al alloy AA5052 and CFRP with polyamide 66 CFRP. In this study, rotating speed and PD were fixed to be 400 rpm and 0.2 mm, respectively. For temperature evaluation at different joining speeds, the experimentally obtained peak temperatures were 474.2 and 486 K with 0.8 and 1 mm/s, respectively. However, the corresponding numerically obtained values were 474.2 and 463.5 K at the same joining speeds. The decrease in peak
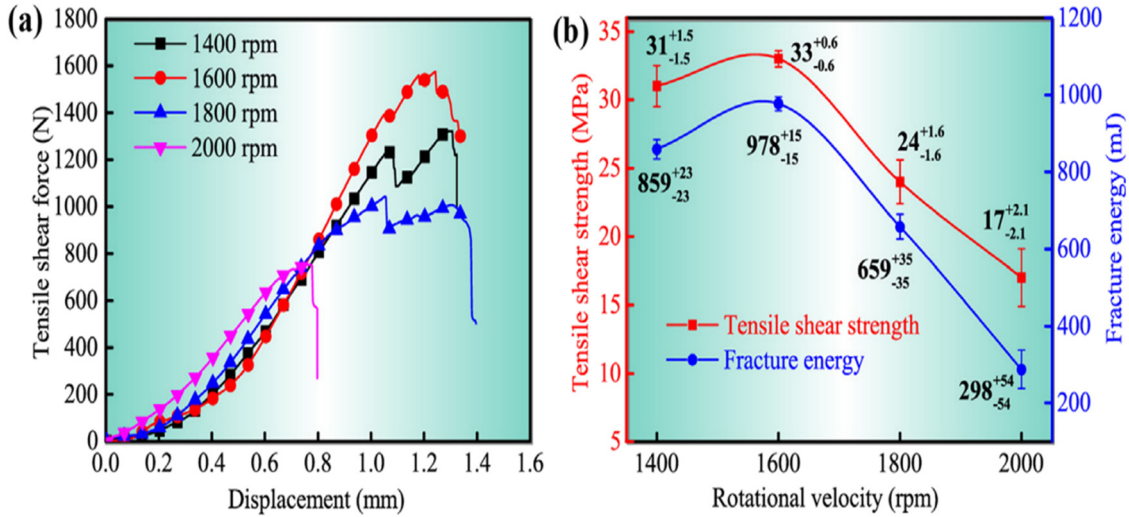
Figure 16: (a) Tensile shear force in different distances and (b) tensile shear strength of hybrid joints at different rotating speeds [240].

temperature is due to the reduction in heat generation in the length joint by increasing joining speed. For the overall joining conditions considered in this study, the prepared samples within a specific range of rotational and joining speeds have exhibited sound bead profiles without any visible discontinuity. Bang *et al.* [242] studied FSW of Al alloy AA5052 and CFRP. In this study, the pinless tool at 400 rpm rotating speed and 0.2 mm plunge was used. The width of the tunnel was increased with an increase in PD. All joints exhibited low strength and failed under the application of force by hand. This can be attributed to hard lower CFRP material, which was not easy for the tool pin to be inserted into CFRP, causing insufficient stirring and frictional heat generation between the upper Al alloy and lower CFRP material. The results showed that the maximum shear force was 2,000 N and strength was 8 MPa. EDS area analysis was further carried out and results

showed that the most significant elements were Al and C with concentrations of 36.18 and 63.82 wt%, respectively. It could be confirmed that the fracture occurred along the joint surface but partially happened between Al alloy and CFRP base material. Ground Al surface acts as locking material to interlock molten CFRP into Al alloy and leads to improve joint strength.

Nagatsuka *et al.* [243] investigated the joining of CFRP with aluminum alloy AA5052 by FSW. The first case used AA5052 as received (unground) whereas the second case used wet grinding with 800 emery papers (ground). The results showed that the tensile shear force of unground Al/carbon fiber was 1 kN, while that of ground Al and CFRP increased significantly and reached 2.9 kN. The tensile shear strength of the joint was decreased with
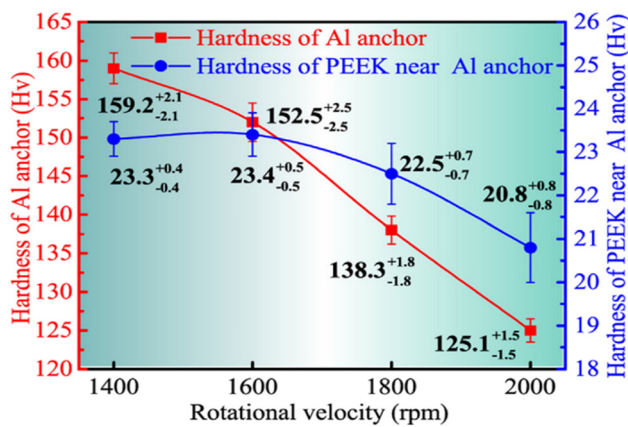

Figure 17: Hardness of typical locations for Al anchor [240].
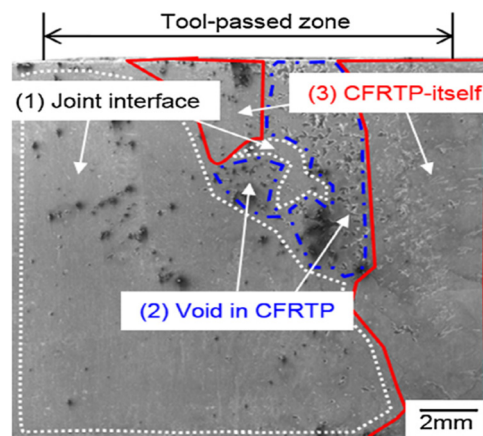

Figure 18: Secondary electron images and classification of fracture surface characteristics on the AA5052 side of fractured joints formed at joining speeds of 1,600 mm min^{-1} [243].

the decrease in the joining speed, regardless of the size of the joined area. The maximum temperatures for ground AA5052 and CFRP were 760 and 725 K at joining speeds of 100 and 1,600 mm/min, respectively, and a fixed PD of 0.9 mm. With the decrease in joining speed, the concave downward deformation of Al was pressed against the underlying CFRP, as shown in Figure 18. The fracture surface of AA5052 in the tool-passed zone was described by three basic characters: joint-interface fracture, void fracture, and CFRP-itself fracture. The area fraction of CFRP itself increased from 0.1 to 55.1% as the joining speed decreased from 2,000 to 100 mm/min.

Hunag *et al.* [244] improved the mechanical properties of joints of Al alloy AA2060-T8 with short carbon-fiber-reinforced PEEK (SCF/PEEK) by FSW. The bonding mechanisms can be divided into electrostatic force for chemical bonding, mechanical interlocking, and physical interaction. In this study, they applied different rotating speeds from 1,400 to 2,000 rpm and used a taper screwed pin at a PD of 0.2 mm. The results showed that maximum micro hardness was 22.6 HV at 1,400 rpm, but tensile shear strength was 18 MPa at 1,600 rpm. Microstructures at different rotating speeds are illustrated in Figure 19. Meanwhile, the low content CFRP easily flows and softens the polymer materials under the rotation of the rotating tool. Under synthesis effects, in the presence of CFRP, there was no obvious influence on tool life.

Franke *et al.* [80] investigated solid-state Al alloy AA6061-T6 and CFRP *via* FSW. Rotating speed was varied in the range of 1,200–2,500 rpm and plunge depth was in the range of 0.2–0.6 mm. The tool was made from H13 steel. Infiltration distances of Al into carbon fiber bed

were measured using the cross-sectional images of samples which showed that plasticized aluminum was modeled as a highly viscous fluid. FSW can melt and displace polymer matrix, plasticize metal constituent, and force it to flow around the fibers. However, a polymer matrix creates space among the fibers and it may be easier for the plasticized metal to flow into that space instead of dry fibers compacted tightly against themselves. Wu *et al.* [1] investigated the mechanical properties of oxygen-free copper and CFRP. Rotating speed was increased from 600 to 2,000 rpm and PD was 0.9 mm. The temperature was measured at the center of each sample, 7.5 mm away from the retreating side and similarly in advancing side (AS) and then 15 mm from the retreating side of the other sample. The results showed that temperatures were 550, 430, 450, and 360°C, respectively, at 1,500 rpm. Maximum tensile shear force was achieved at 1,500 rpm. Joint parameters were enhanced from 0.89–2.25 kN to 1.71–3.54 kN by tool offsetting. During the process, an increase in rotating speed increased the peak temperature. The higher thickness of the re-solidified zone with more bubbles could be due to higher rotation speeds and temperatures. Bubble generation could be described by the fact that when tool was plunged into the copper, CFRP in some specific regions was melted under tool down force. For a high-quality of copper/CFRP welding joint with high tensile shear force and a low number of bubbles, tool offsetting is a good choice, as illustrated in Figure 20.

Wu *et al.* [245] investigated the direct joint of carbon fiber-reinforced thermoplastic and oxygen-free copper by FSW. Rotating speed was fixed at 1,500 rpm and PD was 0.9 mm. The maximum temperature was 350°C and the
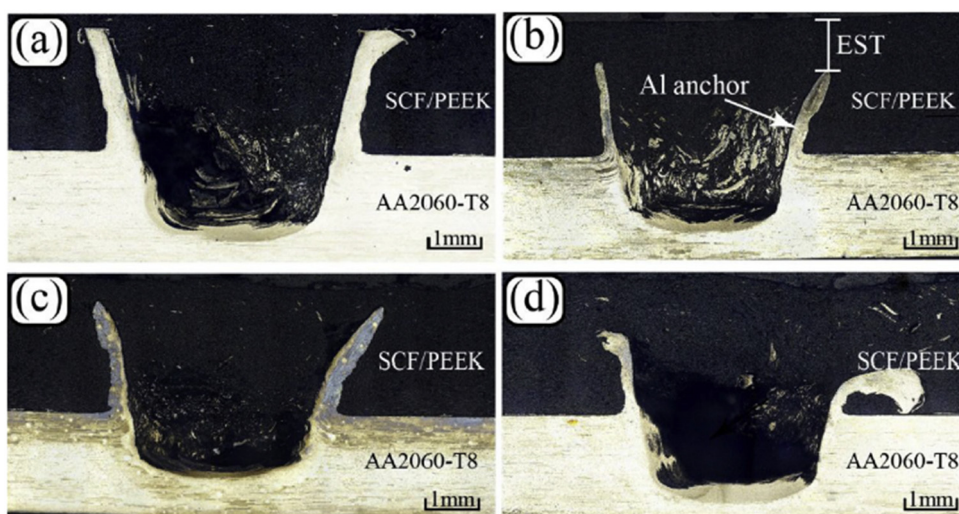

Figure 19: Microstructures at: (a) 1,400 rpm, (b) 1,600 rpm, (c) 1,800 rpm, and (d) 2,000 rpm [244].
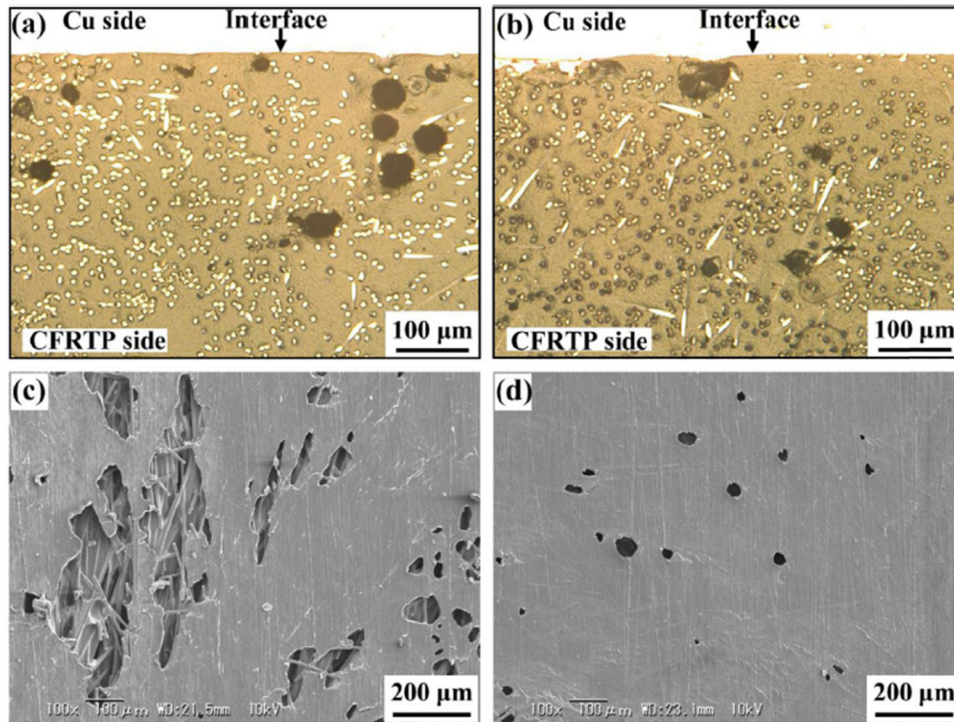
Figure 20: Bubble comparison of normal and offset joints at different rotating speeds and cross-sections: (a) normal friction lap joint at 1,500 rpm, (b) offset joint at 1,500 rpm, (c) normal joint at 2,000 rpm and (d) offset joint at 2,000 rpm [1].

tensile shear force was 2.3 kN, which was mainly affected by the joining area. A large number of bubbles were created due to the melted zone, thermal decomposition of plastic, or air and water vapor. Large joining areas with small degradations generate a small number of bubbles. The fracture would occur along the weakest region of the joint. When there was no joining or the joint bonding was weak enough, the fracture would preferentially occur along with the interface of Cu and CFRP, *i.e.*, adhesive failure. Wang *et al.* [246] investigated FSW of AZ31 magnesium sheet and thermoplastic carbon fiber-reinforced polymer. The tool was made of steel H13 with thread pins. Tool (A) pin length was 2.1 mm with a shoulder of 18 mm and tool (B) was 2 mm long with a 12.7 mm shoulder. When Tool B with a shorter pin length was used at a reduced PD at 800 rpm, the voids in the AS surface of the joint were reduced. The rotating speed was varied from 800 to 1,200 rpm. More heat generation at high RS improved material flow around tool pin. The results showed that average load was 1.87 kN. Maximum microhardness value was 69.9 HV on base AZ31, 57.5 HV on SZ, and 59.3 HV on unmodified interlock. The microhardness of AZ31 is strongly dependent on grain size and larger grain size, typically observed in the SZ/nugget, typically corresponds to lower microhardness. Choi *et al.* [247]

investigated the feasibility of FSW on pure titanium and CFRP. Rotating speed was varied from 50 to 300 rpm at 0.9 mm PD. Argon was applied to avoid oxidation during FSW. Maximum temperature was about 600°C and tensile shear strength out of SZ was 7 kN. This result implies that the silane coupling agent applied on the pure Ti surface cannot react with the CFRP when the interface temperature is lower than the melting point of the CFRP. This is because the FSW process is completed in a short time, thus it is difficult for the molecules of the CFRP and the silane coupling agent to bond with each other when the CFRP and the silane coupling agent are in the solid state. Titanium and CFRP could be completely welded due to sufficiently high friction heat input during FSW.

Lambiase *et al.* [248] studied FSW of carbon fiber and polycarbonate at 0.25 mm PD and 6,000 rpm rotating speed. The results showed high mechanical strength of up to 12 MPa and average temperature of about 300°C. The joints made with PD of 0.05 mm showed a surface in correspondence with the pin path very similar to that of the original CFRP distribution. On the other hand, the joints made with PD of 0.25 mm showed a fragmented surface characterized by sparse fibers over the central region and broken fibers at the side edges of the stirred region. The joints showed delamination failure between

Table 2: Summary of research works on FSW and CFRP with material

No.	Material type and thickness in (mm)		Parameters			Temperature (°C)	Tensile shear force (N)	Type of joint	Ref.
			Rotational speed (rpm)	Dwell time (s)	Travel speed				
1	Carbon fiber/3	AA2060-T8/2	1,400 1,600 1,800 2,000	10–15	30 mm/min	— — — —	1,250 1,550 700 1,000	Single Joint	[240]
2	Carbon fiber/1.5	AA5052/1	400	—	0.8–1 mm/s	213–210	—	Single Joint	[241]
3	Carbon fiber/3	Oxygen-free Cu/2	1,500	—	600 mm/min	≃450	2,300–3,600	Single Joint	[1]
4	Carbon fiber-PA66/1.5 Carbon fiber/1.5	AA5052/2.5 AA5052/1	400	—	0.6–1 mm/s	—	2,000	Single Joint	[242]
5	Carbon fiber/3	AA5052/2	2,000	—	100–1,600 mm/min	452–487	600–4,300	Single Joint	[243]
6	Carbon fiber/3	Oxygen-free Cu/2	1,500	—	200–1,600 mm/min	350	2,300	Single Joint	[245]
7	Carbon fiber/3	AA2060-T8/2	1,400 1,600 1,800 2,000	15	30 mm/min	—	—	Single Joint	[244]
8	Carbon fiber/2	AZ31/2.3	800 –1,200	12	250 mm/min	—	1,870	Single Joint	[246]
9	Carbon fiber/2	Pure Ti/2	50–300	—	100 mm/min	600	7,000	Single Joint	[247]
10	Carbon fiber/1.5	Polycarbonate/3	2,000–6,000	—	10–100 mm/min	180–260	—	Single Joint	[248]

the first and second plies of CFRP. Joints with low PDs showed high strength but low absorbed energy. Lambiase *et al.* [249] investigated the joints of CFRP and amorphous polymers formed by FSW. Rotating and joining speeds were varied in the range of 2,000–6,000 rpm and 10–40 mm/min, respectively. Only one joint was succeeded at 4,000 rpm and 20 mm/min and the others failed between stirred region and polycarbonate base and maximum strength was 17 MPa under optimal conditions. The joints did not fail at the substrates interface; rather, they failed due to CFRP delamination. On the other hand, the joints with the highest strength failed at the boundary of the stirred region and base material. This was due to the presence of bubbles developed between the stirred region and the base material during the process.

Based on the FSW review, the best tensile shear load was 7 kN obtained for pure Ti and CFRP at a RS of 300 rpm and, at a travel speed of 100 mm/min and 0.9 mm PD, the thickness for both pure Ti and CFRP is 2 mm. The interface temperature between the melting point and thermal decomposition points of the CFRP with the simultaneous guarantee of the sufficient duration of the CFRP melt state during FSW is considered to be optimum in terms of the highest tensile shear strength among the examined joints and the fracture at the CFRP matrix outside of the SZ. The summary of research works on FSW and CFRP with material are summarized and presented in Table 2.

6 Summary and future work

The FW of CFRP with sheet metal has fewer concern parameters which have a significant effect on the welding quality. The most efficient parameters are RS, PD, dwell time, and shoulder penetration depth. Through the overview of the presented literature, it has been observed that the RS has a huge impact on the tensile shear load of a FSSW weld joint, as RS increased, the tensile shear load of a CFRP welded joint enhanced. In FSSW, PD is considered as another effective parameter when varying during welding. Results showed that tensile shear load was increased by increasing PD. PD plays a vital role in the interface of the weld joint and establishes an inter-mechanical interlocking between the metal and CFRP weld joint. The increase in PD improves the material flow which leads to an increase in the joint strength of the welded joints. Also, it was found that the best tensile shear load was obtained by CFRP and pure titanium using FSW. In comparison to adhesive-bonded joints, FSSW has provided better weld joint strength. According to the

presented study, by observing the mechanical and microstructure results reached to the level that the FSSW is better than FSW. In the case of different thicknesses of film interlayer, the mechanical performance of a weld joint demonstrates that the joint fabricated with 100 μm interlayers had a high tensile shear force about 3 times greater than the joint with 500 μm. FW material that contains high-temperature properties requires a high dwell time during the welding process to increase heat input and obtain the required temperature, especially in the case of welding high-strength titanium alloys. The material with high melting temperature resulted in low plunge rates and generated sufficient heat to reduce the axial load during the welding process. In FSSW, a keyhole formed at the end of the welding of Al and composite and a reaction layer mostly formed due to the reaction of carbon and oxygen. To overcome the issue of the keyhole, RFSSW has been introduced which can resolve this issue. Even in some cases, it has been observed that during FW, bubbles are produced that can affect the joint strength which can be controlled by increasing the joining area of the weld joint. In some cases, the presence of bubbles had a positive effect on the bonding of CFRP and metal during welding, but after welding, it decreases tensile shear force because of the remaining bubbles. Another factor that got attention during the review of CFRP FW was tool shoulder penetration depth which directly influences the thickness of polycarbonate. Lower shoulder penetration depths resulted in lower thinning of polycarbonate and surface worsening, normally researchers recommend 0.2 mm shoulder penetration to avoid a massive reduction in top metal sheet thickness. A reaction layer composed mostly of metals and CFRP was formed between a metal and re-solidified CFRP inside the hole. While the enhancement of the tool RS did not affect significantly the reaction layer thickness, the weight percent of the metal in this layer increased.

In this article, the authors had conducted a large number of literature studies and reviews. We suggested working on interlayer epically composite material such as CFRP and expected to have a better result on tensile shear load. More researchers should focus on the use of different surface conditions to allow better weld tensile shear load, while a full-scale welding parameter study may also help to identify welding conditions that give improved weld quality. Also, effect of performing welds in the same welding temperature achieved with different combinations of the tool RS and downforce on the material properties.

References

[1] Wu L, Nagatsuka K, Nakata K. Achieving superior mechanical properties in friction lap joints of copper to carbon-fiber-reinforced plastic by tool offsetting. J Mater Sci Technol. 2018;34(9):1628–37.

[2] Liu Z, Li Y, Wang Y, Epureanu BI, Banu M. Nonlinear friction behavior in ultrasonic welding of aluminum alloy to carbon fiber reinforced PA6 composite. J Mater Process Technol. 2021;296:117230.

[3] Wang H, Huang B, Li J, Li N, Liu L. Welding and riveting hybrid bonding of 6061 Al and carbon fiber reinforced composites. Polymers. 2022;14(1):99.

[4] Wippo V, Jaeschke P, Suttmann O, Kaierle S, Overmeyer L. Evaluation of material based influences at laser based heat conduction welding of carbon fiber reinforced plastics. J Mater Process Technol. 2019;31(2):022405.

[5] Chen P, Chen S, Liu H, Peng J, Gao F. The interface behavior of multiple piezoelectric films attaching to a finite-thickness gradient substrate. J Appl Mech. 2020;87(1):011003.

[6] Amancio-Filho ST, Dos Santos JF. Joining of polymers and polymer–metal hybrid structures: recent developments and trends. Polym Eng Sci. 2009;49(8):1461–76.

[7] Chen P, Chen S, Peng J. Interface behavior of a thin-film bonded to a graded layer coated elastic half-plane. Int J Mech Sci. 2016;115:489–500.

[8] Mitschang P, Velthuis R, Didi M. Induction spot welding of metal/CFRPC hybrid joints. Adv Eng Mater. 2013;15(9):804–13.

[9] Wang T, Li L, Pallaka MR, Das H, Whalen S, Soulami A, et al. Mechanical and microstructural characterization of AZ31 magnesium-carbon fiber reinforced polymer joint obtained by friction stir interlocking technique. Mater Des. 2020;198:109305.

[10] Wang X, Morisada Y, Fujii H. Flat friction stir spot welding of AZ31B magnesium alloy using double side adjustable tools: microstructure and mechanical properties. Sci Technol Weld Joining. 2020;25(8):644–52.

[11] Song R, Sahmani S, Safaei B. Isogeometric nonlocal strain gradient quasi-three-dimensional plate model for thermal postbuckling of porous functionally graded microplates with central cutout with different shapes. Appl Math Mech. 2021;42(6):771–86.

[12] Goushegir S. Friction spot joining (FSpJ) of aluminum-CFRP hybrid structures. Weld World. 2016;60(6):1073–93.

[13] Fan F, Lei B, Sahmani S, Safaei B. On the surface elastic-based shear buckling characteristics of functionally graded composite skew nanoplates. Thin-Walled Struct. 2020;154:106841.

[14] Rao R, Sahmani S, Safaei B. Isogeometric nonlinear bending analysis of porous FG composite microplates with a central cutout modeled by the couple stress continuum quasi-3D plate theory. Arch Civ Mech Eng. 2021;21(3):1–17.

[15] Wang P, Yuan P, Sahmani S, Safaei B. Surface stress size dependency in nonlinear free oscillations of FGM quasi-3D nanoplates having arbitrary shapes with variable thickness using IGA. Thin-Walled Struct. 2021;166:108101.

[16] Alibar MY, Safaei B, Asmael M, Zeeshan Q. Effect of carbon nanotubes and porosity on vibrational behavior of nano-composite structures: a review. Arch ComputMethods Eng. 2021;1–37. doi: 10.1007/s11831-021-09669-5.

[17] Kanawade D, Jandali G, Mallick P, editors. Development of thermoplastic matrix composite tubes for automotive applications. Proc 17th Technical Conference of the American Society for Composites. West Lafayette, IN: 2002.

[18] Morgan P. Polymer matrices for carbon fiber composites. Carbon fiber and their composites. New York: Taylor & Francis Group; 2005. p. 534–5.

[19] Wang X, Zhou G, Safaei B, Sahmani S. Boundary layer modeling of surface residual tension in postbuckling behavior of axially loaded silicon panels at nanoscale embedded in elastic foundations. Mech Based Des Struct Mach. 2020;1–18. doi: 10.1080/15397734.2020.1794889.

[20] Qiu J, Sahmani S, Safaei B. On the NURBS-based isogeometric analysis for couple stress-based nonlinear instability of PFGM microplates. Mech Based Des Struct Mach. 2020;1–25. doi: 10.1080/15397734.2020.1853567.

[21] Dong S, Gauvin R. Application of dynamic mechanical analysis for the study of the interfacial region in carbon fiber/epoxy composite materials. Polym Compos. 1993;14(5):414–20.

[22] Sandeep R, Natarajan A. Prediction of peak temperature value in friction lap welding of aluminium alloy 7475 and PPS polymer hybrid joint using machine learning approaches. Mater Lett. 2022;308:131253.

[23] Yang Z, Lu H, Sahmani S, Safaei B. Isogeometric couple stress continuum-based linear and nonlinear flexural responses of functionally graded composite microplates with variable thickness. Arch Civ Mech Eng. 2021;21(3):1–19.

[24] Barbaros I, Yang Y, Safaei B, Yang Z, Qin Z, Asmael M. State-of-the-art review of fabrication, application, and mechanical properties of functionally graded porous nanocomposite materials. Nanotechnol Rev. 2022;11(1):321–71.

[25] Heggemann T, Homberg W. Deep drawing of fiber metal laminates for automotive lightweight structures. Compos Struct. 2019;216:53–7.

[26] Alhijazi M, Safaei B, Zeeshan Q, Asmael M, Eyvazian A, Qin Z. Recent developments in luffa natural fiber composites. Sustainability. 2020;12(18):7683.

[27] Liu Y, Hu W, Zhu R, Safaei B, Qin Z, Chu F. Dynamic responses of corrugated cylindrical shells subjected to nonlinear low-velocity impact. Aerosp Sci Technol. 2022;121:107321.

[28] Pramanik A, Basak A, Dong Y, Sarker P, Uddin M, Littlefair G, et al. Joining of carbon fibre reinforced polymer (CFRP) composites and aluminium alloys–a review. Composites Part A. 2017;101:1–29.

[29] Boucherit A, Abdi S, Aissani M, Mehdi B, Abib K, Badji R. Weldability, microstructure, and residual stress in Al/Cu and Cu/Al friction stir spot weld joints with Zn interlayer. Int J Adv Manuf Technol. 2020;111(5):1553–69.

[30] Safaei B. Frequency-dependent damped vibrations of multi-functional foam plates sandwiched and integrated by composite faces. Eur Phys J Plus. 2021;136(6):1–16.

[31] Yang Z, Safaei B, Sahmani S, Zhang Y. A couple-stress-based moving Kriging meshfree shell model for axial postbuckling analysis of random checkerboard composite cylindrical microshells. Thin-Walled Struct. 2022;170:108631.

[32] Zhang Q, Zhang L, Liu W, Zhang X, Zhu W, Qu S. 3D rigid viscoplastic FE modelling of continuous drive friction welding process. Sci Technol Weld Joining. 2006;11(6):737–43.

[33] Zong K, Qin Z, Chu F. Modeling of frictional stick-slip of contact interfaces considering normal fractal contact. J Appl Mech. 2022;89(3). Paper No: JAM-21-1300.

[34] Uday M, Ahmad Fauzi M, Zuhailawati H, Ismail A. Advances in friction welding process: a review. Sci Technol Weld Joining. 2010;15(7):534–58.

[35] Lambiase F, Grossi V, Paoletti A. High-speed joining of hybrid metal-polymer joints during the friction-assisted joining process. Compos Struct. 2022;280:114890.

[36] Maalekian M. Friction welding–critical assessment of literature. Sci Technol Weld Joining. 2007;12(8):738–59.

[37] Zhang Z, Xiao B, Ma Z. Hardness recovery mechanism in the heat-affected zone during long-term natural aging and its influence on the mechanical properties and fracture behavior of friction stir welded 2024Al–T351 joints. Acta Mater. 2014;73:227–39.

[38] Maalekian M, Kozeschnik E, Brantner HP, Cerjak H. Comparative analysis of heat generation in friction welding of steel bars. Acta Mater. 2008;56(12):2843–55.

[39] Lambiase F, Scipioni SI, Lee C-J, Ko D-C, Liu F. A state-of-the-art review on advanced joining processes for metal-composite and metal-polymer hybrid structures. Materials. 2021;14(8):1890.

[40] Zhao H, Shen Z, Booth M, Wen J, Fu L, Gerlich A. Calculation of welding tool pin width for friction stir welding of thin overlapping sheets. Int J Adv Manuf Technol. 2018;98(5–8):1721–31.

[41] Shen Z, Chen Y, Haghshenas M, Nguyen T, Galloway J, Gerlich A. Interfacial microstructure and properties of copper clad steel produced using friction stir welding versus gas metal arc welding. Mater Charact. 2015;104:1–9.

[42] Rahmat S, Hamdi M, Yusof F, Moshwan R. Preliminary study on the feasibility of friction stir welding in 7075 aluminium alloy and polycarbonate sheet. Mater Res Innovations. 2014;18(Sup6):S6-515–9.

[43] Liu F, Liao J, Nakata K. Joining of metal to plastic using friction lap welding. Mater Des (1980–2015). 2014;54:236–44.

[44] Ratanathavorn W, Melander A. Dissimilar joining between aluminium alloy (AA 6111) and thermoplastics using friction stir welding. Sci Technol Weld Joining. 2015;20(3):222–8.

[45] Li Y, Lu J. Lightweight structure design for wind energy by integrating nanostructured materials. Mater Des. 2014;57:689–96.

[46] Murray RE, Roadman J, Beach R. Fusion joining of thermoplastic composite wind turbine blades: Lap-shear bond characterization. Renewable Energy. 2019;140:501–12.

[47] Shenoi R, Moy SS, Hollaway L. Advanced polymer composites for structural applications in construction. Proceedings of the First International Conference, Held at Southampton University, UK, on 15–17 April 2002. Thomas Telford; 2002.

[48] Guo W, Chen P, Liu H, Yang Y, Peng G, Chen Z. On the strength and interfacial properties of square wave joints with defects and mismatches. J Adhes. 2021;97(13):1211–33.

[49] Dursun T, Soutis C. Recent developments in advanced aircraft aluminium alloys. Mater Des (1980–2015). 2014;56:862–71.

[50] Guo W, Chen P, Yu L, Peng G, Zhao Y, Gao F. Numerical analysis of the strength and interfacial behaviour of adhesively bonded joints with varying bondline thicknesses. Int J Adhes Adhes. 2020;98:102553.

[51] Zhang J, Chaisombat K, He S, Wang CH. Hybrid composite laminates reinforced with glass/carbon woven fabrics for lightweight load bearing structures. Mater Des (1980-2015). 2012;36:75–80.

[52] Singh R, Kumar R, Feo L, Fraternali F. Friction welding of dissimilar plastic/polymer materials with metal powder reinforcement for engineering applications. Composites Part B. 2016;101:77–86.

[53] Khatibi K, Asmael M, Safaei B, Zeeshan Q. Solidification and microstructure characterizations of eutectic aluminum-silicon casting alloy with the addition of tin. Materialwiss Werkstofftech. 2021;52(8):871–8.

[54] Ahmad R, Asmael M. Influence of lanthanum on solidification, microstructure, and mechanical properties of eutectic Al-Si piston alloy. J Mater Eng Perform. 2016;25(7):2799–813.

[55] Ahmad R, Asmael M, Shahizan N, Gandouz S. Reduction in secondary dendrite arm spacing in cast eutectic Al–Si piston alloys by cerium addition. Int J Miner Metall Mater. 2017;24(1):91–101.

[56] Sullivan RA. Automotive carbon fiber: Opportunities and challenges. Jom. 2006;58(11):77–9.

[57] Kumar R, Singh R, Ahuja I, Penna R, Feo L. Weldability of thermoplastic materials for friction stir welding-A state of art review and future applications. Composites Part B. 2018;137:1–15.

[58] Wan Y, Takahashi J. Development of carbon fiber-reinforced thermoplastics for mass-produced automotive applications in Japan. jcompossci. 2021;5(3):86.

[59] Kwon D-J, Kim J-H, Kim Y-J, Kim J-J, Park S-M, Kwon I-J, et al. Comparison of interfacial adhesion of hybrid materials of aluminum/carbon fiber reinforced epoxy composites with different surface roughness. Composites Part B. 2019;170:11–8.

[60] Quilter A. Composites in aerospace applications. IHS White Paper. 2001;444(1):264.

[61]   Liu Y, Zhuang W, Wu S. Damage to carbon fibre reinforced polymers (CFRP) in hole-clinched joints with aluminium alloy and CFRP. Compos Struct. 2020;234:111710.

[62]   Park SY, Choi WJ. 3 Production control effect on composite material quality and stability for aerospace usage. Adv Compos Mater. 2017;112–94.

[63]   Wise R. New technique for joining dissimilar materials. WeldRevInt. 1993;2:40–2.

[64]   Wang S, Liang W, Duan L, Li G, Cui J. Effects of loading rates on mechanical property and failure behavior of single-lap adhesive joints with carbon fiber reinforced plastics and aluminum alloys. Int J Adv Manuf Technol. 2020;106(5):2569–81.

[65]   Lin P-C, Lin J-W, Li G-X. Clinching process for aluminum alloy and carbon fiber-reinforced thermoplastic sheets. Int J Adv Manuf Technol. 2018;97(1–4):529–41.

[66]   Alhijazi M, Safaei B, Zeeshan Q, Asmael M. Modeling and simulation of the elastic properties of natural fiber-reinforced thermosets. Polym Compos. 2021;42:3508–17.

[67]   Messler Jr RW. Joining composite materials and structures: some thought-provoking possibilities. J Thermoplast Compos Mater. 2004;17(1):51–75.

[68]   Zhu W, Xiao H, Wang J, Fu C. Characterization and properties of AA6061-based fiber metal laminates with different aluminum-surface pretreatments. Compos Struct. 2019;227:111321.

[69]   Behrens B-A, Uhe J, Petersen T, Nürnberger F, Kahra C, Ross I, et al. Contact geometry modification of friction-welded semi-finished products to improve the bonding of hybrid components. Metals. 2021;11(1):115.

[70]   Chen P, Chen S, Peng J, Gao F, Liu H. The interface behavior of a thin film bonded imperfectly to a finite thickness gradient substrate. Eng Fract Mech. 2019;217:106529.

[71]   Balle F, Wagner G, Eifler D. Ultrasonic spot welding of aluminum sheet/carbon fiber reinforced polymer – joints. Materialwiss Werkstofftech. 2007;38(11):934–8.

[72]   Balle F, Wagner G, Eifler D. Ultrasonic metal welding of aluminium sheets to carbon fibre reinforced thermoplastic composites. Adv Eng Mater. 2009;11(1–2):35–9.

[73]   Haghshenas M, Khodabakhshi F. Dissimilar friction-stir welding of aluminum and polymer: a review. Int J Adv Manuf Technol. 2019;104(1):333–58.

[74]   Khodabakhshi F, Haghshenas M, Chen J, Shalchi Amirkhiz B, Li J, Gerlich A. Bonding mechanism and interface characterisation during dissimilar friction stir welding of an aluminium/polymer bi-material joint. Sci Technol Weld Joining. 2017;22(3):182–90.

[75]   Alia C, Arenas JM, Suárez JC, Ocana R, Narbón JJ. Mode II fracture energy in the adhesive bonding of dissimilar substrates: carbon fibre composite to aluminium joints. J Adhes Sci Technol. 2013;27(22):2480–94.

[76]   Chowdhury S, Chen D, Bhole S, Cao X, Wanjara P. Lap shear strength and fatigue behavior of friction stir spot welded dissimilar magnesium-to-aluminum joints with adhesive. Mater Sci Eng A. 2013;562:53–60.

[77]   Fink A, Camanho P, Andrés J, Pfeiffer E, Obst A. Hybrid CFRP/titanium bolted joints: Performance assessment and application to a spacecraft payload adaptor. Compos Sci Technol. 2010;70(2):305–17.

[78]   Yan B, Zhu S, Tong M, Pan S. Experimental study on the mechanical properties of laminates made of thin carbon fiber plies. Compos Struct. 2020;245:112336.

[79]   Lambiase F, Balle F, Blaga L-A, Liu F, Amancio-Filho ST. Friction-based processes for hybrid multi-material joining. Compos Struct. 2021;266:113828.

[80]   Franke DJ, Morrow JD, Zinn MR, Pfefferkorn FE. Solid-state infiltration of 6061-T6 aluminum alloy into carbon fibers via friction stir welding. J Manuf Sci Eng. 2017;139(11). Paper No: MANU-16-1649.

[81]   Ma N, Geng P, Ma Y, Shimakawa K, Choi J-W, Aoki Y, et al. Thermo-mechanical modeling and analysis of friction spot joining of Al alloy and carbon fiber-reinforced polymer. J Mater Res Technol. 2021;12:1777–93.

[82]   Davies P, Cantwell W, Jar P-Y, Bourban P-E, Zysman V, Kausch H. Joining and repair of a carbon fibre-reinforced thermoplastic. Composites. 1991;22(6):425–31.

[83]   Jiang B, Chen Q, Yang J. Advances in joining technology of carbon fiber-reinforced thermoplastic composite materials and aluminum alloys. Int J Adv Manuf Technol. 2020;110:1–19.

[84]   Lambiase F, Paoletti A, Durante M. Mechanism of bonding of AA7075 aluminum alloy and CFRP during friction assisted joining. Compos Struct. 2021;261:113593.

[85]   Jeon C-S, Jeong Y-H, Hong S-T, Hasan MT, Tien HN, Hur S-H, et al. Mechanical properties of graphite/aluminum metal matrix composite joints by friction stir spot welding. J Mech Sci Technol. 2014;28(2):499–504.

[86]   Beylergil B, Tanoğlu M, Aktaş E. Effect of polyamide-6, 6 (PA 66) nonwoven veils on the mechanical performance of carbon fiber/epoxy composites. Compos Struct. 2018;194:21–35.

[87]   Huang Y, Meng X, Wang Y, Xie Y, Zhou L. Joining of aluminum alloy and polymer via friction stir lap welding. J Mater Process Technol. 2018;257:148–54.

[88]   Huang Y, Meng X, Xie Y, Li J, Wan L. New technique of friction-based filling stacking joining for metal and polymer. Composites Part B. 2019;163:217–23.

[89]   Meng X, Huang Y, Xie Y, Li J, Guan M, Wan L, et al. Friction self-riveting welding between polymer matrix composites and metals. Composites Part A. 2019;127:105624.

[90]   Lang F, Xing Y, Zhao Y, Zhu J, Hou X, Zhang W. Experimental determination of the interface residual stresses of carbon-fiber-reinforced polymers. Compos Struct. 2020;254:112849.

[91]   Bilici MK, Yükler A, Kurtulmuş M. The optimization of welding parameters for friction stir spot welding of high density polyethylene sheets. Mater Des. 2011;32(7):4074–9.

[92]   Yusof F, Muhamad MRB, Moshwan R, Jamaludin MFB, Miyashita Y. Effect of surface states on joining mechanisms and mechanical properties of aluminum alloy (A5052) and polyethylene terephthalate (PET) by dissimilar friction spot welding. Metals. 2016;6(5):101.

[93]   Arici A, Mert Ş. Friction stir spot welding of polypropylene. J Reinf Plast Compos. 2008;27(18):2001–4.

[94]   Dashatan SH, Azdast T, Ahmadi SR, Bagheri A. Friction stir spot welding of dissimilar polymethyl methacrylate and acrylonitrile butadiene styrene sheets. Mater Des. 2013;45:135–41.

[95]   Oliveira P, Amancio-Filho S, Dos Santos J, Hage Jr E. Preliminary study on the feasibility of friction spot welding in PMMA. Mater Lett. 2010;64(19):2098–101.

[96] Chen P, Chen S, Guo W, Gao F. The interface behavior of a thin piezoelectric film bonded to a graded substrate. Mech Mater. 2018;127:26–38.

[97] Su P, Gerlich A, North T, Bendzsak G. Intermixing in dissimilar friction stir spot welds. Metall Mater Trans A. 2007;38(3):584–95.

[98] Behrens B-A, Chugreev A, Matthias T, Nothdurft S, Hermsdorf J, Kaierle S et al., editors. Investigation of the composite strength of hybrid steel-steel semi-finished products manufactured by laser beam welding and friction welding. 5th International Conference Recent Trends in Structural Materials 1416 November 2018, Pilsen, Czech Republic.

[99] Gerlich A, Su P, North T. Peak temperatures and microstructures in aluminium and magnesium alloy friction stir spot welds. Sci Technol Weld Joining. 2005;10(6):647–52.

[100] Adithya P, Sunil B, Kumar CL. Optimization of process parameters for friction stir spot welding using dissimilar metals. Intelligent manufacturing and energy sustainability. Singapore: Springer; 2022. p. 185–97.

[101] Lambiase F, Grossi V, Scipioni S, Paoletti A. Prediction of the power supplied in friction-based joining process of metal-polymer hybrids through machine learning. J Manuf Processes. 2021;68:750–60.

[102] Esteves JV, Goushegir S, dos Santos JF, Canto LB, Hage Jr E, Amancio-Filho S. Friction spot joining of aluminum AA6181-T4 and carbon fiber-reinforced poly (phenylene sulfide): Effects of process parameters on the microstructure and mechanical strength. Mater Des. 2015;66:437–45.

[103] André NM. Friction spot joining of aluminum alloy 2024-t3 and carbon-fiber-reinforced polyphenylene sulfide composite laminate with additional pps film interlayer. [Master thesis]; 2015.

[104] Herbst S, Aengeneyndt H, Maier HJ, Nürnberger F. Microstructure and mechanical properties of friction welded steel-aluminum hybrid components after T6 heat treatment. Mater Sci Eng A. 2017;696:33–41.

[105] Goushegir S, Dos Santos J, Amancio-Filho S. Influence of process parameters on mechanical performance and bonding area of AA2024/carbon-fiber-reinforced poly (phenylene sulfide) friction spot single lap joints. Mater Des. 2015;83:431–42.

[106] Kumar RD, Muthukumaran S, Venkateswaran T, Xavier V, Sivakumar D. Failure analysis and process parameter influence on mechanical and metallurgical behavior of friction stir welded Aa2219-T87 joints. Surf Rev Lett. 2020;27(2):1950107.

[107] André NM, Goushegir SM, Santos J, Canto LB, Amancio-Filho ST, editors. On the microstructure and mechanical performance of Friction Spot Joining with additional film interlayer. Proceedings of the Annual Technical Conference of Society of Plastics Engineers (ANTEC 2014). USA: Society of Plastics Engineers; 2014.

[108] Paoletti A, Lambiase F, Di, Ilio A. Optimization of friction stir welding of thermoplastics. Procedia CIRP. 2015;33:562–7.

[109] Su P, Gerlich A, North T, Bendzsak G. Energy generation and stir zone dimensions in friction stir spot welds. SAE Trans. 2006;115:717–25.

[110] Asmael M, Glaissa M. Effects of rotation speed and dwell time on the mechanical properties and microstructure of dissimilar aluminum-titanium alloys by friction stir spot welding (FSSW). Materialwiss Werkstofftech. 2020;51(7):1002–8.

[111] Schmidt HB, Hattel JH. Thermal modelling of friction stir welding. Scr Mater. 2008;58(5):332–7.

[112] Su P, Gerlich A, North T. Friction stir spot welding of aluminum and magnesium alloy sheets. SAE Technical Paper; 2005. Report No.: 0148-7191.

[113] Gerlich A, Avramovic-Cingara G, North T. Stir zone microstructure and strain rate during Al 7075-T6 friction stir spot welding. Metall Mater Trans A. 2006;37(9):2773–86.

[114] Gerlich A, Yamamoto M, North T. Strain rates and grain growth in Al 5754 and Al 6061 friction stir spot welds. Metall Mater Trans A. 2007;38(6):1291–302.

[115] Zhang L, Zhang F, Qin Z, Han Q, Wang T, Chu F. Piezoelectric energy harvester for rolling bearings with capability of self-powered condition monitoring. Energy. 2022;238:121770.

[116] Paidar M, Khodabandeh A, Najafi H, Rouh-aghdam AS. Retracted article: an investigation on mechanical and metallurgical properties of 2024-T3 aluminum alloy spot friction welds. Int J Adv Manuf Technol. 2015;80(1–4):183–97.

[117] Bozzi S, Helbert-Etter A, Baudin T, Klosek V, Kerbiguet J, Criqui B. Influence of FSSW parameters on fracture mechanisms of 5182 aluminium welds. J Mater Process Technol. 2010;210(11):1429–35.

[118] Mitlin D, Radmilovic V, Pan T, Chen J, Feng Z, Santella M. Structure–properties relations in spot friction welded (also known as friction stir spot welded) 6111 aluminum. Mater Sci Eng A. 2006;441(1–2):79–96.

[119] Xu L, Wang L, Chen Y-C, Robson JD, Prangnell PB. Effect of interfacial reaction on the mechanical performance of steel to aluminum dissimilar ultrasonic spot welds. Metall Mater Trans A. 2016;47(1):334–46.

[120] Bakavos D, Prangnell P. Effect of reduced or zero pin length and anvil insulation on friction stir spot welding thin gauge 6111 automotive sheet. Sci Technol Weld Joining. 2009;14(5):443–56.

[121] Shen Z, Yang X, Zhang Z, Cui L, Yin Y. Mechanical properties and failure mechanisms of friction stir spot welds of AA 6061-T4 sheets. Mater Des. 2013;49:181–91.

[122] Nasir T, Kalaf O, Asmael M. Effect of rotational speed, and dwell time on the mechanical properties and microstructure of dissimilar AA5754 and AA7075-T651 aluminum sheet alloys by friction stir spot welding. Mater Sci. 2021;27:308–12.

[123] Yusof F, Miyashita Y, Seo N, Mutoh Y, Moshwan R. Utilising friction spot joining for dissimilar joint between aluminium alloy (A5052) and polyethylene terephthalate. Sci Technol Weld Joining. 2012;17(7):544–9.

[124] Prangnell PB, Bakavos D, editors. Novel approaches to friction spot welding thin aluminium automotive sheet. Materials Science Forum. Vol. 638. Switzerland: Trans Tech Publications; 2010. p. 1237–42.

[125] Abed BH, Salih OS, Sowoud KM. Pinless friction stir spot welding of aluminium alloy with copper interlayer. Open Eng. 2020;10(1):804–13.

[126] Chen Y, Liu S, Bakavos D, Prangnell P. The effect of a paint bake treatment on joint performance in friction stir spot welding AA6111-T4 sheet using a pinless tool. Mater Chem Phys. 2013;141(2–3):768–75.

[127] Bakavos D, Chen Y, Babout L, Prangnell P. Material interactions in a novel pinless tool approach to friction stir spot welding thin aluminum sheet. Metall Mater Trans A. 2011;42(5):1266–82.

[128] Aota K, Ikeuchi K. Development of friction stir spot welding using rotating tool without probe and its application to low-carbon steel plates. Weld Int. 2009;23(8):572–80.

[129] Gerlich A, Su P, North T. Tool penetration during friction stir spot welding of Al and Mg alloys. J Mater Sci. 2005;40(24):6473–81.

[130] Tozaki Y, Uematsu Y, Tokaji K. A newly developed tool without probe for friction stir spot welding and its performance. J Mater Process Technol. 2010;210(6–7):844–51.

[131] Reilly A, Shercliff H, Chen Y, Prangnell P. Modelling and visualisation of material flow in friction stir spot welding. J Mater Process Technol. 2015;225:473–84.

[132] Xu R, Ni D, Yang Q, Liu C, Ma Z. Pinless friction stir spot welding of Mg–3Al–1Zn alloy with Zn interlayer. J Mater Sci Technol. 2016;32(1):76–88.

[133] Shen Z, Yang X, Zhang Z, Cui L, Li T. Microstructure and failure mechanisms of refill friction stir spot welded 7075-T6 aluminum alloy joints. Mater Des. 2013;44:476–86.

[134] Kubit A, Bucior M, Wydrzyński D, Trzepieciński T, Pytel M. Failure mechanisms of refill friction stir spot welded 7075-T6 aluminium alloy single-lap joints. Int J Adv Manuf Technol. 2018;94(9–12):4479–91.

[135] Shen Z, Yang X, Yang S, Zhang Z, Yin Y. Microstructure and mechanical properties of friction spot welded 6061-T4 aluminum alloy. Mater Des (1980–2015). 2014;54:766–78.

[136] Kolba T, Faes K, De Waele W. Experimental investigation of the weldability of high strength aluminium using friction spot welding. Int J Sustainable Constr Des. 2016;7(1):8. doi: 10.2185/scad.v7i1.3638.

[137] Plaine A, Suhuddin U, Alcântara N, Dos Santos J. Fatigue behavior of friction spot welds in lap shear specimens of AA5754 and Ti6Al4V alloys. Int J Fatigue. 2016;91:149–57.

[138] Junior WS, Handge UA, dos Santos JF, Abetz V, Amancio-Filho ST. Feasibility study of friction spot welding of dissimilar single-lap joint between poly (methyl methacrylate) and poly (methyl methacrylate)-SiO2 nanocomposite. Mater Des. 2014;64:246–50.

[139] Yu G, Chen X, Zhang B, Pan K, Yang L. Tensile-shear mechanical behaviors of friction stir spot weld and adhesive hybrid joint: experimental and numerical study. Metals. 2020;10(8):1028.

[140] Reis PN, Amaro A, Loureiro A. Comparison of mechanical performance between friction-stir spot welded and adhesive bonded joints. Frattura ed Integrità Strutturale. 2020;14(53):124–33.

[141] André NM, Goushegir SM, Dos Santos JF, Canto LB, Amancio-Filho ST. Friction Spot Joining of aluminum alloy 2024-T3 and carbon-fiber-reinforced poly (phenylene sulfide) laminate with additional PPS film interlayer: Microstructure, mechanical strength and failure mechanisms. Composites Part B. 2016;94:197–208.

[142] Goushegir S, Dos Santos J, Amancio-Filho S. Friction spot joining of aluminum AA2024/carbon-fiber reinforced poly (phenylene sulfide) composite single lap joints: microstructure and mechanical performance. Mater Des (1980–2014). 2015;54:196–206.

[143] Manente André NF, Dos Santos JT, Amancio-Filho S. Evaluation of joint formation and mechanical performance of the AA7075-T6/CFRP spot joints produced by frictional heat. Materials. 2019;12(6):891.

[144] Manente André N, Goushegir SM, Scharnagl N, dos Santos JF, Canto LB, Amancio-Filho ST. Composite surface pre-treatments: Improvement on adhesion mechanisms and mechanical performance of metal–composite friction spot joints with additional film interlayer. J Adhes. 2018;94(9):723–42.

[145] André NM, Goushegir SM, dos Santos JF, Canto LB, Amancio-Filho ST. Influence of the interlayer film thickness on the mechanical performance of AA2024-T3/CF-PPS hybrid joints produced by friction spot joining. Weld Int. 2018;32(1):1–10.

[146] Ogawa Y, Akebono H, Tanaka K, Sugeta A. Effect of welding time on fatigue properties of friction stir spot welds of Al to carbon fibre-reinforced plastic. Sci Technol Weld Joining. 2019;24(3):235–42.

[147] Ogawa Y, Xiong Y, Akebono H, Kato M, Tanaka K, Sugeta A. Fatigue properties of friction stir welds of treated Al to carbon fibre-reinforced plastic. Sci Technol Weld Joining. 2018;23(1):79–86.

[148] Amancio-Filho S, Bueno C, Dos Santos J, Huber N, Hage Jr E. On the feasibility of friction spot joining in magnesium/fiber-reinforced polymer composite hybrid structures. Mater Sci Eng A. 2011;528(10–11):3841–8.

[149] Gonçalves J, Dos Santos J, Canto L, Amancio-Filho S. Friction spot welding of carbon fiber-reinforced polyamide 66 laminate. Mater Lett. 2015;159:506–9.

[150] Huang Y, Meng X, Xie Y, Lv Z, Wan L, Cao J, et al. Friction spot welding of carbon fiber-reinforced polyetherimide laminate. Compos Struct. 2018;189:627–34.

[151] Gonçalves J, dos Santos JF, Canto LB, Filho STA. Improvement of friction spot welding (FSpW) to join polyamide 6 and polyamide 66/carbon fibre laminate. Weld Int. 2016;30(4):247–54.

[152] Bolouri A, Fotouhi M, Moseley W. A new design for friction stir spot joining of Al alloys and carbon fiber-reinforced composites. J Mater Eng Perform. 2020;29:1–9.

[153] Nasir T, Kalaf O, Asmael M, Zeeshan Q, Safaei B, Hussain G, et al. The experimental study of CFRP interlayer of dissimilar joint AA7075-T651/Ti-6Al-4V alloys by friction stir spot welding on mechanical and microstructural properties. Nanotechnol Rev. 2021;10(1):401–13.

[154] Kalaf O, Nasir T, Asmael M, Safaei B, Zeeshan Q, Motallebzadeh A, et al. Friction stir spot welding of AA5052 with additional carbon fiber-reinforced polymer composite interlayer. Nanotechnol Rev. 2021;10(1):201–9.

[155] Schilling C, dos Santos J. Method and device for joining at least two adjoining work pieces by friction welding. Google Patents; 2004.

[156] Tier M, Rosendo T, Olea C, Mazzaferro C, Ramos F, Bayer M et al. editors. The influence of weld microstructure on mechanical properties of refill friction spot welding of 5042 aluminium alloy. 7th International Friction Stir Welding Symposium. Japan: SAE Technical Papers Awaji Island; 2008.

[157] Shen Z, Ding Y, Chen J, Fu L, Liu X, Chen H, et al. Microstructure, static and fatigue properties of refill friction stir spot welded 7075-T6 aluminium alloy using a modified tool. Sci Technol Weld Joining. 2019;24(7):587–600.

[158] Larsen BA. Increasing the manufacturing readiness of refill friction stir spot welding. [Theses and Dissertations Master of Science]. USA: Brigham Young University; 2020.

[159] Ashong AN, Lee M, Hong S-T, Lee YS, Kim JH. Refill friction stir spot welding of dissimilar AA6014 Al alloy and carbon-fiber-reinforced polymer composite. Met Mater Int. 2021;27(4):639–49.

[160] Suhuddin U, Fischer V, Dos Santos J. The thermal cycle during the dissimilar friction spot welding of aluminum and magnesium alloy. Scr Mater. 2013;68(1):87–90.

[161] Rosendo T, Parra B, Tier M, Da Silva A, Dos Santos J, Strohaecker T, et al. Mechanical and microstructural investigation of friction spot welded AA6181-T4 aluminium alloy. Mater Des. 2011;32(3):1094–100.

[162] Shen Z, Ding Y, Gopkalo O, Diak B, Gerlich A. Effects of tool design on the microstructure and mechanical properties of refill friction stir spot welding of dissimilar Al alloys. J Mater Process Technol. 2018;252:751–9.

[163] Shen Z, Chen J, Ding Y, Hou J, Shalchi Amirkhiz B, Chan K, et al. Role of interfacial reaction on the mechanical performance of Al/steel dissimilar refill friction stir spot welds. Sci Technol Weld Joining. 2018;23(6):462–77.

[164] Schmal C, Meschut G. Refill friction stir spot and resistance spot welding of aluminium joints with large total sheet thicknesses (III-1965-19). Weld World. 2020;64:1471–80.

[165] Allen CD, Arbegast WJ. Evaluation of friction spot welds in aluminum alloys. SAE Trans. 2005;114:612–8.

[166] Nasiri AM, Shen Z, Hou JSC, Gerlich AP. Failure analysis of tool used in refill friction stir spot welding of Al 2099 alloy. Eng Fail Anal. 2018;84:25–33.

[167] Dong H, Chen S, Song Y, Guo X, Zhang X, Sun Z. Refilled friction stir spot welding of aluminum alloy to galvanized steel sheets. Mater Des. 2016;94:457–66.

[168] Shen Z, Ding Y, Chen J, Amirkhiz BS, Wen J, Fu L, et al. Interfacial bonding mechanism in Al/coated steel dissimilar refill friction stir spot welds. J Mater Sci Technol. 2019;35(6):1027–38.

[169] Chen Y, Chen J, Shalchi Amirkhiz B, Worswick M, Gerlich A. Microstructures and properties of Mg alloy/DP600 steel dissimilar refill friction stir spot welds. Sci Technol Weld Joining. 2015;20(6):494–501.

[170] Plaine A, Suhuddin U, Afonso C, Alcântara N, Dos Santos J. Interface formation and properties of friction spot welded joints of AA5754 and Ti6Al4V alloys. Mater Des. 2016;93:224–31.

[171] Shen J, Suhuddin UF, Cardillo ME, dos Santos JF. Eutectic structures in friction spot welding joint of aluminum alloy to copper. Appl Phys Lett. 2014;104(19):191901.

[172] Patnaik A, Koch K, Arbegast W, Allen C. Static properties of "refill" friction spot welded skin stiffened compression panels. SAE Technical Paper; 2006. Report No.: 0148-7191.

[173] Dracup BJ, Arbegast WJ. Friction stir welding as a rivet replacement technology. SAE Technical Paper; 1999. Report No.: 0148-7191.

[174] Kubit A, Wydrzynski D, Trzepiecinski T. Refill friction stir spot welding of 7075-T6 aluminium alloy single-lap joints with polymer sealant interlayer. Compos Struct. 2018;201:389–97.

[175] Lacki P, Derlatka A. Strength evaluation of beam made of the aluminum 6061-T6 and titanium grade 5 alloy sheets joined by RFSSW and RSW. Compos Struct. 2017;159:491–7.

[176] Cox CD, Gibson BT, Strauss AM, Cook GE. Effect of pin length and rotation rate on the tensile strength of a friction stir spot-welded Al alloy: a contribution to automated production. Mater Manuf Processes. 2012;27(4):472–8.

[177] Tozaki Y, Uematsu Y, Tokaji K. Effect of tool geometry on microstructure and static strength in friction stir spot welded aluminium alloys. Int J Mach Tools Manuf. 2007;47(15):2230–6.

[178] Shen Z, Li W, Ding Y, Hou W, Liu X, Guo W, et al. Material flow during refill friction stir spot welded dissimilar Al alloys using a grooved tool. J Manuf Processes. 2020;49:260–70.

[179] Cao J, Zhang C, Xing Y, Wang M. Pin plunging reinforced refill friction stir spot welding of Alclad 2219 to 7075 alloy. J Mater Process Technol. 2020;284:116760.

[180] Montag T, Wulfsberg J-P, Hameister H, Marschner R. Influence of tool wear on quality criteria for refill friction stir spot welding (RFSSW) process. Procedia CIRP. 2014;24:108–13.

[181] Ji S, Wang Y, Li Z, Yue Y, Chai P. Effect of tool geometry on material flow behavior of refill friction stir spot welding. Trans Indian Inst Met. 2017;70(6):1417–30.

[182] Pabandi HK, Movahedi M, Kokabi AH. A new refill friction spot welding process for aluminum/polymer composite hybrid structures. Compos Struct. 2017;174:59–69.

[183] Ashong AN, Lee M, Hong S-T, Lee YS, Kim JH. Refill friction stir spot welding of dissimilar AA6014 Al alloy and carbon-fiber-reinforced polymer composite. Met Mater Int. 2020;27:1–11.

[184] Goushegir SM, Scharnagl N, dos Santos JF, Amancio-Filho ST. XPS analysis of the interface between AA2024-T3/CF-PPS friction spot joints. Surf Interface Anal. 2016;48(8):706–11.

[185] Özel T, Karpat Y, Srivastava A. Hard turning with variable micro-geometry PcBN tools. CIRP annals. 2008;57(1):73–6.

[186] Ramachandran K, Murugan N, Kumar SS. Effect of tool axis offset and geometry of tool pin profile on the characteristics of friction stir welded dissimilar joints of aluminum alloy AA5052 and HSLA steel. Mater Sci Eng A. 2015;639:219–33.

[187] Suri A. An improved FSW tool for joining commercial aluminum plates. Proc Mater Sci. 2014;6:1857–64.

[188] Shah LHA, Sonbolestan S, Midawi AR, Walbridge S, Gerlich A. Dissimilar friction stir welding of thick plate AA5052-AA6061 aluminum alloys: effects of material positioning and tool eccentricity. Int J Adv Manuf Technol. 2019;105(1–4):889–904.

[189] Mehta KP, Badheka VJ. Influence of tool design and process parameters on dissimilar friction stir welding of copper to AA6061-T651 joints. Int J Adv Manuf Technol. 2015;80(9–12):2073–82.

[190] Sharifitabar M, Nami H. Microstructures of dissimilar friction stir welded joints between 2024-T4 aluminum alloy and Al/Mg2Si metal matrix cast composite. Composites Part B. 2011;42(7):2004–12.

[191] Yang X, Zhang H, Dong P, Yan Z, Wang W. A study on the formation of multiple intermetallic compounds of friction stir processed high entropy alloy particles reinforced Al matrix composites. Mater Charact. 2022;183:111646.

[192] Wang Z, Zhang J, Xie G, Wu L, Zhang H, Xue P, et al. Evolution mechanisms of microstructure and mechanical properties in a friction stir welded ultrahigh-strength quenching and partitioning steel. J Mater Sci Technol. 2022;102:213–23.

[193] Meng X, Huang Y, Cao J, Shen J, dos Santos JF. Recent progress on control strategies for inherent issues in friction stir welding. Prog Mater Sci. 2020;115:100706.

[194] Uzun H, Dalle Donne C, Argagnotto A, Ghidini T, Gambaro C. Friction stir welding of dissimilar Al 6013-T4 to X5CrNi18-10 stainless steel. Mater Des. 2005;26(1):41–6.

[195] Gibson BT, Lammlein D, Prater T, Longhurst W, Cox C, Ballun M, et al. Friction stir welding: process, automation, and control. J Manuf Processes. 2014;16(1):56–73.

[196] Thomas W, Nicholas E. Friction stir welding for the transportation industries. Mater Des. 1997;18(4–6):269–73.

[197] Williams SW. Welding of airframes using friction stir. Air Space Europe. 2001;3(3–4):64–6.

[198] Kumar R, Singh R, Ahuja I, Amendola A, Penna R. Friction welding for the manufacturing of PA6 and ABS structures reinforced with Fe particles. Composites Part B. 2018;132:244–57.

[199] Mishra RS, Ma Z. Friction stir welding and processing. Mater Sci Eng R Rep. 2005;50(1–2):1–78.

[200] Wu L, Xiao B, Nagatsuka K, Nakata K, Ma Z. Achieving strong friction lap joints of carbon-fiber reinforced plastic and metals by modifying metal surface structure via laser-processing pretreatment. Compos Struct. 2020;242:112167.

[201] Krishnan K. On the formation of onion rings in friction stir welds. Mater Sci Eng A. 2002;327(2):246–51.

[202] Kimapong K, Watanabe T. Friction stir welding of aluminum alloy to steel. Welding J. 2004;83(10):277.

[203] Anand R, Sridhar V. Studies on process parameters and tool geometry selecting aspects of friction stir welding–A review. Mater Today Proc. 2020;27:576–83.

[204] Kumar S, Roy BS. Novel study of joining of acrylonitrile butadiene styrene and polycarbonate plate by using friction stir welding with double-step shoulder. J Manuf Processes. 2019;45:322–30.

[205] Abdulmalik S, Ahmad R, Asmael M, editors. Surface modification of hypereutectic Al-Si alloy via friction stir process. AIP Conference Proceedings. AIP Publishing LLC; 2017.

[206] Soori M, Asmael M, Solyalı D. Recent development in friction stir welding process: a review. SAE Int J Mater Manuf. 2020;16:63–80.

[207] Yasui T, Tsubaki M, Fukumoto M, Shimoda Y, Ishii T. High-speed weldability between 6063 and S45C by friction stir welding. Study of welding of dissimilar metals by friction stir welding (1st report). Weld Int. 2006;20(4):284–9.

[208] Messler RW. Joining comes of age: from pragmatic process to enabling technology. Assembly automation. Vol. 23. MCB UP Ltd. UK: Emerald Publishing Limited; 2003. p. 130–143.

[209] Arora A, Dien BS, Belyea RL, Singh V, Tumbleson ME, Rausch KD. Nutrient recovery from the dry grind process using sequential micro and ultrafiltration of thin stillage. Bioresour Technol. 2010;101(11):3859–63.

[210] Peel M, Steuwer A, Preuss M, Withers P. Microstructure, mechanical properties and residual stresses as a function of welding speed in aluminium AA5083 friction stir welds. Acta Mater. 2003;51(16):4791–801.

[211] Glaissa MAA, Asmael M, Zeeshan Q. Recent applications of residual stress measurement techniques for FSW. Joints A J Kejuruteraan. 2020;32(3):1–15.

[212] McKnight SH, Holmes ST, Gillespie Jr JW, Lambing CL, Marinelli JM. Scaling issues in resistance-welded thermoplastic composite joints. Adv Polym Technol. 1997;16(4):279–95.

[213] Tauqir N, Mohammed A, Qassim Z, Davut S. Applications of machine learning to friction stir welding process optimization. A J Kejuruteraan. 2020;32(1):171–86.

[214] Yalavarthy H. Friction stir welding process and material microstructure evolution modeling in 2,000 and 5,000 series of aluminum alloys [Thesis]. USA: Clemson University Pro Quest Dissertations Publishing; 2009.

[215] Cao X, Shi Q, Liu D, Feng Z, Liu Q, Chen G. Fabrication of in situ carbon fiber/aluminum composites via friction stir processing: evaluation of microstructural, mechanical and tribological behaviors. Composites Part B. 2018;139:97–105.

[216] Behrens B-A, Chugreev A, Selinski M, Matthias T, editors. Joining zone shape optimisation for hybrid components made of aluminium-steel by geometrically adapted joining surfaces in the friction welding process. 22nd international Esaform Confrence On Material Forming, 8 May 2019. AIP Publishing LLC; 2019.

[217] Krasnowski K, Hamilton C, Dymek S. Influence of the tool shape and weld configuration on microstructure and mechanical properties of the Al 6082 alloy FSW joints. Arch Civ Mech Eng. 2015;15(1):133–41.

[218] Kusuda Y. Honda develops robotized FSW technology to weld steel and aluminum and applied it to a mass-production vehicle. Industrial Robot Int J. 2013;40(3):208–12.

[219] Haghshenas M, Gerlich A. Joining of automotive sheet materials by friction-based welding methods: a review. Eng Sci Technol Int J. 2018;21(1):130–48.

[220] Chen Y, Nakata K. Effect of tool geometry on microstructure and mechanical properties of friction stir lap welded magnesium alloy and steel. Mater Des. 2009;30(9):3913–9.

[221] Haghshenas M, Abdel-Gwad A, Omran A, Gökçe B, Sahraeinejad S, Gerlich A. Friction stir weld assisted diffusion bonding of 5754 aluminum alloy to coated high strength steels. Mater Des. 2014;55:442–9.

[222] Qiu R, Iwamoto C, Satonaka S. The influence of reaction layer on the strength of aluminum/steel joint welded by resistance spot welding. Mater Charact. 2009;60(2):156–9.

[223] Singh R, Kumar V, Feo L, Fraternali F. Experimental investigations for mechanical and metallurgical properties of friction stir welded recycled dissimilar polymer materials with metal powder reinforcement. Composites Part B. 2016;103:90–7.

[224] Gerlich A, Yamamoto M, Shibayanagi T, North T. Selection of welding parameter during friction stir spot welding. SAE Int J Mater Manuf. 2009;1(1):1–8.

[225] Rao H, Jordon J, Barkey M, Guo Y, Su X, Badarinarayan H. Influence of structural integrity on fatigue behavior of friction stir spot welded AZ31 Mg alloy. Mater Sci Eng A. 2013;564:369–80.

[226] Kurt HI. Influence of hybrid ratio and friction stir processing parameters on ultimate tensile strength of 5083 aluminum matrix hybrid composites. Composites Part B. 2016;93:26–34.

[227] Khosa SU, Weinberger T, Enzinger N. Thermo-mechanical investigations during friction stir spot welding (FSSW) of AA6082-T6. Weld World. 2010;54(5–6):R134–46.

[228] Saunders N, Miles M, Hartman T, Hovanski Y, Hong S-T, Steel R. Joint strength in high speed friction stir spot welded DP 980 steel. Int J Precis Eng Manuf. 2014;15(5):841–8.

[229] Lathabai S, Painter M, Cantin G, Tyagi V. Friction spot joining of an extruded Al–Mg–Si alloy. Scr Mater. 2006;55(10):899–902.

[230] Fujimoto M, Koga S, Abe N, Sato SY, Kokawa H. Analysis of plastic flow of the Al alloy joint produced by friction stir spot welding. Weld Int. 2009;23(8):589–96.

[231] Fujimoto M, Inuzuka M, Koga S, Seta Y. Development of friction spot joining. Weld World. 2005;49(3–4):18–21.

[232] Paidar M, Tahani K, Vignesh RV, Ojo O, Ezatpour H, Moharrami A. Modified friction stir clinching of 2024-T3 to 6061-T6 aluminium alloy: effect of dwell time and precipitation-hardening heat treatment. Mater Sci Eng A. 2020;791:139734.

[233] Gemme F, Verreman Y, Dubourg L, Jahazi M. Numerical analysis of the dwell phase in friction stir welding and comparison with experimental data. Mater Sci Eng A. 2010;527(16–17):4152–60.

[234] Gerlich A, Yamamoto M, North TH. Local melting and tool slippage during friction stir spot welding of Al-alloys. J Mater Sci. 2008;43(1):2–11.

[235] De Leon M, Shin H-S. Material flow behaviours during friction stir spot welding of lightweight alloys using pin and pinless tools. Sci Technol Weld Joining. 2016;21(2):140–6.

[236] Sun Z, Wu C. Influence of tool thread pitch on material flow and thermal process in friction stir welding. J Mater Process Technol. 2020;275:116281.

[237] Hirasawa S, Badarinarayan H, Okamoto K, Tomimura T, Kawanami T. Analysis of effect of tool geometry on plastic flow during friction stir spot welding using particle method. J Mater Process Technol. 2010;210(11):1455–63.

[238] Gadakh VS, Adepu K. Heat generation model for taper cylindrical pin profile in FSW. J Mater Res Technol. 2013;2(4):370–5.

[239] Dialami N, Cervera M, Chiumenti M. Effect of the tool tilt angle on the heat generation and the material flow in friction stir welding. Metals. 2019;9(1):28.

[240] Huang Y, Meng X, Xie Y, Li J, Wan L. Joining of carbon fiber reinforced thermoplastic and metal *via* friction stir welding with co-controlling shape and performance. Composites Part A. 2018;112:328–36.

[241] Das A, Bang H, editors. Numerical modelling in friction lap joining of aluminium alloy and carbon-fiber-reinforced-plastic sheets. IOP Conference Series Mater Sci Eng. IOP Publishing; 2018.

[242] Bang H, Das A, Lee S, editors. Friction stir lap joining of automotive aluminium alloy and carbon-fiber-reinforced plastic. IOP Conference Series Mater Sci Eng. IOP Publishing; 2018.

[243] Nagatsuka K, Yoshida S, Tsuchiya A, Nakata K. Direct joining of carbon-fiber–reinforced plastic to an aluminum alloy using friction lap joining. Composites Part B. 2015;73:82–8.

[244] Huang Y, Meng X, Xie Y, Li J, Si X, Fan Q. Improving mechanical properties of composite/metal friction stir lap welding joints *via* a taper-screwed pin with triple facets. J Mater Process Technol. 2019;268:80–6.

[245] Wu L, Nagatsuka K, Nakata K. Direct joining of oxygen-free copper and carbon-fiber-reinforced plastic by friction lap joining. J Mater Sci Technol. 2018;34(1):192–7.

[246] Wang T, Upadhyay P, Reza-E-Rabby M, Li X, Li L, Soulami A, et al. Joining of thermoset carbon fiber reinforced polymer and AZ31 magnesium alloy sheet *via* friction stir interlocking. Int J Adv Manuf Technol. 2020;109:1–10.

[247] Choi J-W, Morisada Y, Liu H, Ushioda K, Fujii H, Nagatsuka K, et al. Dissimilar friction stir welding of pure Ti and carbon fibre reinforced plastic. Sci Technol Weld Joining. 2020;25:1–9.

[248] Lambiase F, Grossi V, Di Ilio A, Paoletti A. Feasibility of friction stir joining of polycarbonate to CFRP with thermosetting matrix. Int J Adv Manuf Technol. 2020;106(5):2451–62.

[249] Lambiase F, Grossi V, Paoletti A. Friction Stir Joining of CFRP laminates with amorphous polymers: influence of processing speeds. J Manuf Processes. 2020;55:186–97.